



# Assessment of the Nuclear Risk in Europe - A case Study in the Almaraz NPP Spain

*A study performed in the framework of a collaboration agreement  
between the EC JRC and CIEMAT*

Hernandez Ceballos, M., Trueba Alonso, C., Garcia  
Puerta, B., Sangiorgi, M., Montero Prieto, M., De Felice, L.

2024

This document is a publication by the Joint Research Centre (JRC), the European Commission's science and knowledge service. It aims to provide evidence-based scientific support to the European policymaking process. The contents of this publication do not necessarily reflect the position or opinion of the European Commission. Neither the European Commission nor any person acting on behalf of the Commission is responsible for the use that might be made of this publication. For information on the methodology and quality underlying the data used in this publication for which the source is neither Eurostat nor other Commission services, users should contact the referenced source. The designations employed and the presentation of material on the maps do not imply the expression of any opinion whatsoever on the part of the European Union concerning the legal status of any country, territory, city or area or of its authorities, or concerning the delimitation of its frontiers or boundaries.

**EU Science Hub**

<https://joint-research-centre.ec.europa.eu>

JRC128119

EUR 31038 EN

PDF ISBN 978-92-76-51139-7 ISSN 1831-9424 doi:10.2760/02698

KJ-NA-31038-EN-N

Luxembourg: Publications Office of the European Union, 2024

© European Atomic Energy Community, 2024



The reuse policy of the European Commission documents is implemented by the Commission Decision 2011/833/EU of 12 December 2011 on the reuse of Commission documents (OJ L 330, 14.12.2011, p. 39). Unless otherwise noted, the reuse of this document is authorised under the Creative Commons Attribution 4.0 International (CC BY 4.0) licence (<https://creativecommons.org/licenses/by/4.0/>). This means that reuse is allowed provided appropriate credit is given and any changes are indicated.

For any use or reproduction of photos or other material that is not owned by the European Atomic Energy Community permission must be sought directly from the copyright holders.

How to cite this report: European Commission, Joint Research Centre, Hernandez Ceballos, M.A., Trueba Alonso, C., Garcia Puerta, B., Sangiorgi, M., Montero Prieto, M. and De Felice, L., *Assessment of the Nuclear Risk in Europe - A case Study in the Almaraz NPP, Spain*, Publications Office of the European Union, Luxembourg, 2024, <https://data.europa.eu/doi/10.2760/02698>, JRC128119.

# Contents

Abstract .....	2
Foreword.....	3
Acknowledgements .....	4
Executive summary.....	5
1 Introduction.....	8
2 Objectives.....	10
3 Methodology .....	11
3.1 Hazard identification.....	12
3.2 Estimation of effects and consequences of the release.....	12
3.2.1 Meteorological characterisation.....	12
3.2.2 Atmospheric dispersion simulation.....	13
3.2.3 Deposition analysis.....	13
3.3 Vulnerability assessment.....	14
3.4 Prioritisation maps .....	14
4 Case study: Almaraz NPP .....	15
4.1 Almaraz NPP characteristics.....	15
4.2 Meteorological characterisation.....	16
4.2.1 Local-scale wind and precipitation patterns.....	16
4.2.2 Regional-scale wind patterns .....	17
4.3 Estimation of effects and consequences of the release.....	18
4.3.1 Atmospheric dispersion simulations.....	18
4.3.2 Deposition maps .....	22
4.4 Vulnerability Assessment .....	23
4.5 Identification of prioritisation areas: nuclear risk maps .....	26
5 Discussion and Conclusions .....	29
6 Dissemination of project results .....	32
References .....	35
List of abbreviations and definitions .....	38
List of figures .....	39
List of tables.....	40
Annexes .....	41
Annex 1. Density maps calculation.....	41
Annex 2. Methodology to identify and characterize the dispersion and ground deposition of radioactive material according to airflow patterns .....	44
Annex 3. ISLOCA AND LTSBO source terms adapted to Almaraz NPP.....	48
Annex 4. Meteorological data.....	50
Annex 5. RIMPUFF ADM and EmergencyLite simulation.....	51
Annex 6 Post-processing and visualization of the results from JRODOS.....	56

## **Abstract**

The uncontrolled release of radionuclides in the atmosphere caused by a nuclear or radiological accident may affect large areas, having an effect, not only on public health, but also on the economy because of the restrictions on food production and therefore, the way of life of the affected population. The risk posed by these kind of releases, at any specific place, is a function of several factors, such as the amount and composition of the radionuclides released, the atmospheric dispersion and deposition pattern, the radiological vulnerability of the affected area (in terms of its potentiality to transfer the contamination to the population), the socioeconomic structures affected (number of persons potentially exposed, land use restrictions) and the policies that may affect the afore mentioned.

The elaboration of risk maps, as tools to identify and categorise the affected areas in terms of radiological impact to population, are very useful in Emergency Preparedness and Response Plans, as they allow to prioritise where the application of remediation techniques is necessary. The ANURE project (Assessment of the Nuclear Risk in Europe - A Case Study in the Almaraz Nuclear Power Plant, Spain) has developed a methodology to elaborate this type of risk maps, integrating all the factors previously considered, in order to identify the areas of most concern. The European Commission Joint Research Centre (EC JRC) and the Centro de Investigaciones Energéticas Medioambientales y Tecnológicas (CIEMAT) led this project.

## **Foreword**

The CIEMAT (Centro de Investigaciones Energéticas, Medioambientales y Tecnológicas) and the JRC (Joint Research Centre) of the European Commission have expressed their mutual desire to co-operate in various areas of nuclear research. This collaboration has an emphasis on nuclear safety and for that purpose, the Collaboration Agreement (CA) JRC/CIEMAT nº 34231 dated 13/01/2016, between both institutions was signed (JRC: ARES (2016) 292303-20/01/2016; CIEMAT: 6467/2014).

The general objective of the signed CA is to contribute more effectively to understand and resolve issues in the nuclear field, leading to more effective management techniques and strategies to improve nuclear safety.

Under the precise Area of Emergency Preparedness and Radioprotection a Specific Agreement (SA) was signed, with the purpose to develop the project ANURE "Assessment of the Nuclear Risk in Europe - A Case Study in the Almaraz Nuclear Power Plant (Spain)". The project has been aimed at developing a methodology to elaborate nuclear risk maps, considering local factors, to be used by decision-makers in the preparedness and management of a nuclear post-accident exposure situation.

The Spanish Almaraz NPP was taken as reference on which to apply the methodology developed, which is based on the simulation, from five consecutive years, of the dispersion calculations of two different source terms, i) a severe accident with a relatively large release and ii) a severe accident with small release. The deposit probability obtained as output, combined with detailed information of the soil vulnerability and the food chain impact, provides an estimation of the risk distribution associated with both kinds of nuclear releases in terms of prioritisation maps, which allow to identify and to categorise those areas where the application of remediation techniques is necessary.

The present report describes the whole set of work performed, the methodology defined and the main analysis and results obtained in the framework of this collaboration. For the sake of clarity, it is important to note that these results are in the context of training and testing the methodology, and therefore, further analysis (e.g. source terms, meteorological data, ...) should be performed to use them as reference in the nuclear Emergency Preparedness and Response (EP&R) framework.

## **Acknowledgements**

The authors want to acknowledge the CIEMAT and the JRC of the European Commission for the opportunity to carry out this Project in the frame of the respective Collaboration Agreement (<sup>1</sup>) and Specific Agreement (<sup>2</sup>).

Acknowledgements are also given to the Karlsruhe Institute of Technology (KIT) as manager of the JRODOS Decision Support System for the support given on the use of the system and the Air Resources Laboratory from National Oceanic and Atmospheric Administration (NOAA, U.S. Department of Commerce) for the provision of the HYSPLIT transport and dispersion model used in this publication.

Also, thanks the Spanish Meteorological Agency (AEMET) and the KIT JRODOS Team for the support given to analyse and visualize with JRODOS the meteorological forecast data obtained from the HIRLAM and HARMONIE numerical models; NOAA is also acknowledged as manager of the Global Forecast System (GFS) from which the meteorological data used for the simulations has been obtained.

The authors acknowledge the ENEN PLUS Project for supporting Blanca García Puerta's mobility grant for a three-month research stay at the JRC-Ispra, during 2019.

Finally, the editor also like to thank Manuel Martín Ramos (EC JRC) and Pilar García Ibañez (CIEMAT) for their respective institutional support in making the results of the ANURE project available to the research community and Ursula Carvajal (JRC) first and Juan Carlos Brul (JRC) later for their efforts and help with the administrative arrangements for the production of this publication.

## **Authors**

European Commission, Joint Research Centre, Ispra Italy:

Miguel Angel Hernández Ceballos,

Marco Sangiorgi,

Luca De Felice.

Department of Environment, CIEMAT, Madrid, Spain:

Cristina Trueba Alonso,

Blanca García Puerta,

Milagros Montero Prieto.

## **Editor**

Milagros Montero Prieto, Research Centre for Energy, Environment and Technology (CIEMAT), Department of Environment, Radiation Protection of Public and Environment Unit, Madrid, ES.

---

(<sup>1</sup>) Collaboration Agreement (CA) JRC/CIEMAT nº 34231.

(<sup>2</sup>) ANURE Project "Assessment of the Nuclear Risk in Europe - A Case Study in the Almaraz Nuclear Power Plant (Spain)".

## **Executive summary**

The atmospheric dispersion of uncontrolled released radionuclides may affect large areas at any specific place. Although any deposit may pose a radiological risk, in the case of affecting agricultural areas, it is important to take into account that different agricultural systems show different vulnerabilities to transfer the deposited contamination through the food chain exposure pathway. The combination of the deposition pattern with the soil-to-crop transfer vulnerability, allows the estimation of the radiological risk to the exposure through the food chain pathway. The risk mapping helps to identify and categorise the affected areas according to their potential radiological impact becoming a useful tool in the framework of the Emergency Preparedness and Response (EP&R) to make decisions to prioritise where to act and to design the adequate recovery strategy planning. The ANURE project (Assessment of the NUclear Risk in Europe - A Case Study in the Almaraz Nuclear Power Plant, Spain) develops a methodology to elaborate these maps and applies it in a case study at the Almaraz Nuclear Power Plant.

## **Policy context**

This work is framed within the European Union Council Directive 2013/59, which establishes the basic safety standards for protection against the dangers arising from exposure to ionising radiation and more specifically both in the emergency preparedness and in the establishment of strategies to ensure the appropriate management of existing exposure situations after an emergency exposure situation.

## **Key conclusions**

The ANURE methodology has been shown to successfully address the assessment of radiological risk through the food chain exposure pathway, derived from a release of radionuclides to environment following a nuclear power plant accident.

The methodology developed provides an innovative contribution to EP&R by integrating two complementary approaches, considering the probability and severity of deposition resulting from an accidental radionuclide release with the susceptibility of the soil to transfer the deposited activity concentration along the food chain exposure pathway, resulting in a categorisation of affected areas according to the radiological risk posed by food chain exposure.

The risk maps produced can help to anticipate and assess the potential off-site consequences of such accidental releases, providing a useful decision-making tool for planning protection and recovery strategies and identifying priority areas for action.

The more effective and precise the assessment of the consequences, the better the response of the measures to be applied, and the smaller the uncertainties.

The results of the case study highlight the importance of taking into account local specificities and of having sufficient information in advance of a radiological or nuclear event to produce accurate risk maps.

It is shown that for a given accident, the dispersion and deposition patterns are strongly influenced by the prevailing meteorological conditions and orographic features. Similarly, the radiological vulnerability associated with a soil-plant system is strongly influenced by local soil characteristics, land use and existing crops. Therefore, high deposition levels do not directly imply a higher radiological risk; it is necessary to know the transfer potential of the activity concentration to the crop in order to properly assess the risk.

The methodology can be applicable to any European spot and could also be appropriate for nuclear disaster risk assessment approaches in the context of a National Risk Assessment that covers risks of natural, anthropogenic and socio-natural origin.

## **Main findings**

Risk maps can be useful tools in the preparedness stage of the emergency management cycle as guidance in the decision-making process to reduce the consequences of a severe nuclear accident and to plan the recovery of the affected areas.

A methodology has been developed to map the risk of radiological exposure via the food chain pathway in the event of a severe nuclear accident with off-site consequences, taking into account the deposition of released radionuclides and the soil susceptibility to transfer of the activity concentration deposited along the food chain.

For this purpose, an indicator-based approach consisting of two components has been developed. The first component is a deposition map taking into account the dispersion simulations of the released radionuclides, the estimation of their soil deposition pattern and the severity of the contamination in the environment. The numerical dispersion calculations in this type of risk analysis are based on the generation of release plumes for many possible meteorological conditions, so that the statistical results reflect the deposition patterns in terms of probability of occurrence weighted by severity of deposition. The second component assesses and maps the intrinsic radiological vulnerability of agricultural land through indicators of the influence of soil characteristics on the transfer potential of activity concentration from soil to crop to entry into the food chain. The combination of the two results allows to categorise and map contaminated areas according to their radiological risk and to identify those where remediation measures should be applied as a matter of priority.

A case study on the  $^{137}\text{Cs}$  deposition in rainfed cereals following an ISLOCA accident at the Almaraz NPP in Spain has been used as a reference to test the methodology. However, this can be applied to other nuclear sites where an accidental event with off-site consequences has taken place, provided information on both soil deposition and soil-to-crop vulnerability are available.

Using  $^{137}\text{Cs}$  as representative radionuclide for the source term released, the deposition pattern obtained, that follows a South West-North East axis, affecting with different degree of severity the Iberian Peninsula, is in agreement with the density map simulated for that same period in which the barrier effect of the orography has an important distribution. The results also show the effect of the seasonal meteorological conditions in the likelihood of occurrence and the severity of the radioactive deposition on the environment.

In the other way, the spatial distribution of the vulnerability is determined by the clay content and potassium status in soils and the crop capacity to uptake radiocaesium, measured by means of a transfer factor (TF). The maps produced show that the areas with higher vulnerabilities are those in which concur low clay content and potassium reservoir in soils and high TF values.

A prioritisation map is obtained from the combination of both outcomes, which categorises the agricultural areas where rainfed cereals are grown, attending to the probability to be contaminated with  $^{137}\text{Cs}$  and their radiological vulnerability, and identifying those where the recovery actions should be applied in a prioritised way. Risk maps express the magnitude and geographic distribution of the affected area providing support on where, when and how to implement the possible recovery strategies to minimise the risk.

### ***Related and future work***

According to the outcomes obtained in the developing ANURE project, several assessments may be set to enlarge the tools to be applied in the EP&R, regarding a severe nuclear accident management in Europe. Adapting all the input parameters to the European area would be a must; in that sense, European soil properties maps, published by the European Soil Data Centre (ESDAC)<sup>3</sup>, could be relevant as baseline data in future tasks. Those tasks would be focussed on including other radionuclides which would pose a risk for the food chain, such as  $^{90}\text{Sr}$ . Defining the radiological vulnerability and priority to act regarding different crops, even for products from livestock practices all around Europe, constitute a research line to be continued.

Evaluating the deposition patterns derived from accidental releases from the European NPPs (considering diverse types of nuclear accidents) would be necessary to perform the deposition maps and elaborate the prioritisation maps in each EU region.

Analysing the ingestion doses received from consuming food produced in areas affected by a potential deposition is another approach raised during the ANURE project. It would be highly interesting to be addressed in further research.

These results would contribute to generate scientific knowledge and could facilitate an informed, effective and optimised decision-making process in an accidental event, focused on minimising the radionuclides transfer to the food chain.

### ***Quick guide***

The report explains the purpose and objective of the methodology developed to assess nuclear risk by means of maps that identify and categorise the areas more likely to cause a radiological risk through the food chain exposure pathway. The methodological approach considered combines both dispersion and deposition simulations and soil-to-crop vulnerability assessments.

---

<sup>(3)</sup> <https://esdac.jrc.ec.europa.eu/>

A special focus is dedicated to a case study that tests this development, which shows the usefulness of the risk maps in the preparedness stage of the emergency management cycle, especially as guide during the decision-making process to plan recovery strategies.

The files with the simulations' outputs are available to be downloaded in the JRC repository:

<https://data.jrc.ec.europa.eu/collection/id-00336>

## 1 Introduction

The uncontrolled release of radionuclides to the environment may occur as a result of a nuclear or radiological (N/R) accident (IAEA, 2005), and can affect areas not only in the vicinity of the release point, but also far away, transcending national boundaries (e.g. Sevelyeva and Panchenko, 2012; Steinhauser et al., 2014). The potential contamination of large agricultural areas and semi-natural ecosystems, due to the accumulation of radionuclides in soils, and their transfer through the food chain exposure pathway can give rise to consequences that threaten not only public health and ecological systems, they can have also important socioeconomic implications, because of the restrictions on the land use or production and therefore, the living conditions of the affected population. This circumstance will trigger national and international efforts to reduce its occurrence and to minimize health, environmental and economic impacts.

Already during the early phase of an emergency associated to a large-scale accident with release of radioactive material, it is not only essential to notify the competent authorities as early and efficiently as possible, but also to exchange relevant radiological information promptly. Only timely information on the (likely) extension and evolution of the radioactive contamination on the impacted area can lead to sound proper coordinated response actions to protect the affected population and environment. Following in the next phases, at the post-accident, the assessment of the radiological consequences and the adequate planning, development and management of recovery strategies are required to facilitate the rehabilitation of the contaminated area and the timely resumption of normal living conditions.

Adequate preparedness is the basis for responding to these challenges. Therefore, the European Basic Safety Standards for protection against the dangers arising from exposure to ionising radiation<sup>4</sup> require the effective management of the N/R emergencies, to be addressed by a prior preparedness phase in which "...emergency response plans are established in advance for the various types of emergencies identified by an assessment of potential emergency exposure situations...", including "provision for the transition from an emergency exposure situation to an existing exposure situation", where it will then be necessary to undertake the recovery and long-term rehabilitation tasks.

As early as 2010, the OCDE Nuclear Energy Agency (NEA) published a framework of key considerations for the emergency planning and preparedness (OECD/NEA, 2010), in which it was noted that the first steps in the planning stage will be to undertake a threat and risk assessment. This assessment would help to identify the range of impacts that might occur within the country or abroad and their potential consequences, allowing to derive the types of scenarios of concern for which detailed plans and capabilities should be elaborated, including the development of protection strategies for the early response phase as well as for consequence management and transition to recovery.

In the same line, the Council Conclusions on Further Developing Risk Assessment for Disaster Management within the European Union (2011)<sup>5</sup> emphasized the importance of risk assessment for the integrated disaster risk management at the national level. The procedure, as it has been standardised<sup>6</sup>, is the overall process of risk identification, risk analysis, and risk evaluation. It enhances the basis for the analysis of prevention and preparedness measures as well as for capacity analysis and capability planning, and is a continuous and necessary building block for the development of a coherent risk management policy. (Poljansek et al., 2022).

Regarding to the accidental radioactive releases, the risk assessment approach can be complex due to the number of factors to be considered, such as:

- the likelihood of a large-scale release of radionuclides from nuclear facilities;
- the amount and composition of the radionuclides released (source term);
- the atmospheric dispersion and deposition pattern (meteorological conditions);
- the radiological vulnerability of the affected area (in terms of its potentiality to transfer the contamination to the population);

(<sup>4</sup>) Council Directive 2013/59/EURATOM, of 5 December 2013, laying down basic safety standards for protection against the dangers arising from exposure to ionising radiation, and repealing Directives 89/618/Euratom, 90/641/Euratom, 96/29/Euratom, 97/43/Euratom and 2003/122/Euratom. Official Journal of the European Union, L 13, 17.1.2014, 1-73.  
<https://eur-lex.europa.eu/eli/dir/2013/59/2014-01-17>

(<sup>5</sup>) Council conclusions on Further Developing Risk Assessment for Disaster Management within the European Union, adopted by the Justice and Home Affairs Council on 11-12 April 2011  
[https://www.consilium.europa.eu/uedocs/cms\\_data/docs/pressdata/en/jha/121462.pdf](https://www.consilium.europa.eu/uedocs/cms_data/docs/pressdata/en/jha/121462.pdf)

(<sup>6</sup>) International Organization for Standardization. ISO 31010:2018 Risk management – Risk assessment techniques

- the socioeconomic structures affected (number of persons potentially exposed, land use restrictions); and
- the policies that may affect the afore-mentioned.

Risk mapping has been endorsed by the EU Council as one of the ways to support the risk assessment process<sup>7</sup>, by providing the information on hazards, consequences, vulnerabilities, presenting the outputs of risk analysis in a given area, and helping to define and prioritise risk reduction strategies.

In the broader context of EP&R, N/R risk maps can help to better represent and make available in advance the extent and magnitude of the off-site consequences of potential accidental releases of radioactive materials from nuclear power plants, they could help to identify and categorise the most affected areas and where the application of remediation techniques to mitigate the consequences might be feasible and effective, with the view to restoring normal living conditions as far as possible. Finally, they also have an important role to play in ensuring that all those involved in risk assessment have the same information about the hazards and in disseminating the results of risk assessment to stakeholders.

In the past, several studies have discussed possible approaches and explored some of the important issues mentioned above. However, since the adoption of risk assessment as a formalised analytical process and, more recently, as a policy tool to support regulatory decision making, there has been an increase in projects that have developed or are developing more complex methodologies for estimating risk and/or vulnerability to accidental radioactive releases in conjunction with risk mapping. Examples include the Ar-NARP project (Baklanov, 2003), NordRisk I and II (Lauritzen, 2007 and 2011, respectively), global risk studies (Lelieveld et al., 2012 and Christoudias et al., 2014) or the flexRISK project (Seibert et al., 2013).

Among the more recent projects, the ANURE project (Assessment of the NUclear Risk in Europe - A Case Study in the Almaraz Nuclear Power Plant, Spain) proposes a methodology for the preparation of maps describing the radiological risk through the food chain exposure pathway derived from the release of radionuclides into the environment following a nuclear power plant accident. This project was developed in collaboration between the Spanish Energy, Environmental and Technological Research Centre (Centro de Investigaciones Energéticas, Medioambientales y Tecnológicas - CIEMAT) and the Joint Research Centre (JRC) of the European Commission<sup>8</sup>. The present report presents all the work carried out in the framework of this collaboration, the methodology defined and the main findings and outcomes of the case study used to train the methodological approach.

---

(<sup>7</sup>) Commission [Staff Working Paper on Risk Assessment and Mapping Guidelines for Disaster Management](#), 21 December 2010, 17833/10, SEC(2010) 1626 which was welcomed by the related EU Council conclusions on Further Developing Risk Assessment for Disaster Management within the European Union (see the previous footnote).

(<sup>8</sup>) Collaboration Agreement (CA) JRC/CIEMAT nº 34231

## 2 Objectives

The project ANURE “Assessment of the Nuclear Risk in Europe - A Case Study in the Almaraz Nuclear Power Plant (Spain)” (2017 – 2019), has been developed in the framework of the generic collaboration agreement between the CIEMAT (Centro de Investigaciones Energéticas, Medioambientales y Tecnológicas) and the JRC (Joint Research Centre) of the European Commission to contribute more effectively to understand and resolve issues in the nuclear field, leading to more effective management techniques and strategies to improve nuclear safety in the precise Area of Emergency Preparedness and Radioprotection.

The **main objective** of the project was to develop a methodology to contribute to the assessment and mapping of nuclear risk in Europe, in particular to describe the radiological risk through the food chain exposure pathway resulting from the release and deposition of radionuclides in the environment following an accident in a nuclear power plant, taking into account local factors, and which could be used by decision makers in preparing for and managing a nuclear exposure situation following an accident.

This include the following **specific objectives**:

- To assess the off-site radiological consequences of severe NPP accidents, taking into account the different meteorological conditions that influence the patterns of radionuclide dispersion and deposition, their accumulation in soils and their transfer to plants according to the soil parameters that influence soil vulnerability,
- To develop a methodology to determine the geographical distribution of risk from severe accidents in European NPPs.
- To train the methodology by developing a case study in a Spanish nuclear power plant.

In addition, the project has aimed to promote cooperation in understanding and solving nuclear EP&R issues from a multidisciplinary perspective, to develop methodologies and promote methods to end-users, to exchange appropriate scientific knowledge in nuclear EP&R and to identify knowledge gaps in the analysis, quantification and communication of nuclear risk assessment.

The **results** can be used in the framework of the EP& R to categorise and map contaminated areas according to their radiological risk and to identify those where remediation measures should be applied as a matter of priority. The outcomes of ANURE will provide comprehensive and locally oriented information to decision makers to enable the adequate planning, and to develop and manage recovery strategies.

ANURE foresees the use of several tools for this purpose. The HYSPLIT model (Stein et al., 2015) to compute air mass trajectories providing a reliable characterization of the wind patterns at the selected region and estimating the behaviour of the dispersion. The numerical dispersion calculations have been carried out using the JRODOS System (Realtime Online DecisiOn Support system) (KIT, 2017), for a defined accidental scenario as well as the deposition maps. Finally, the vulnerability and prioritisation maps have been developed using GIS tools (ESRI, 2016).

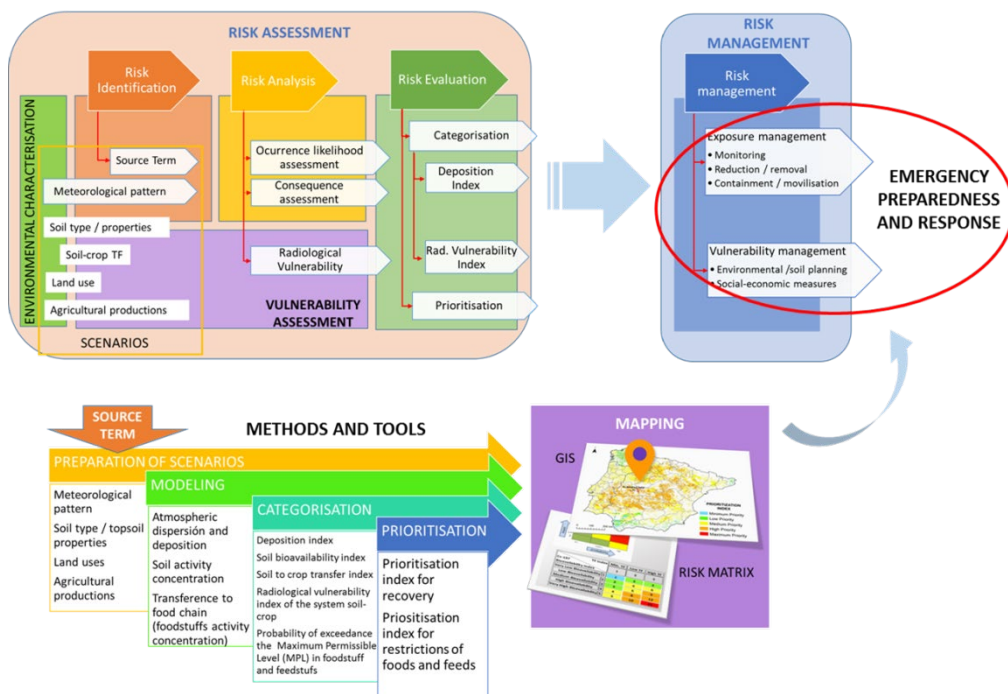
### 3 Methodology

The ANURE project proposes a methodology for the elaboration of nuclear risk maps through the food chain exposure pathway derived from an accidental release of radioactive material, combining a source of contamination, understood as a radionuclide deposition on the soil and the soil potential to make it bioavailable through the food exposure pathway, that is, the soil vulnerability.

The figure 1 shows each step and element considered in the methodological design in relation to the general process of risk assessment and mapping (as it is described in Poljansek et al., 2022).

The first step is to contextualise the problem and identify the risk. The purpose of **risk identification** is to find, recognise and describe risks. Adequate and realistic prioritisation maps must take into account the location and characteristics of the radioactive release, the prevailing meteorological conditions affecting dispersion and deposition, and a detailed knowledge of the potentially affected area, including the soil properties, land use or agricultural practices that determine the behaviour of radionuclides in soils and their transfer to the food chain. With all this information, the **scenarios** of potential risk situations to be assessed are constructed.

**Figure 1.** Methodological design of the risk assessment and mapping processes in ANURE.



Source: Own elaboration. CIEMAT, 2022.

In the next stage of **risk analysis** the level of risk for each scenario is determined by combining the components of the risk, i.e. **hazard, exposure** and **vulnerability**. Once the hazard has been identified, its dispersion and deposition are determined by the source term emitted and the prevailing meteorological conditions at the time of the emission. To obtain the most probable soil deposition pattern, a series of numerical atmospheric dispersion simulations, for a time period, are considered. Soil contamination levels combined with the probability of its occurrence can denote the severity of the radiation exposure associated to such deposition pattern. The consequences are defined as the cumulative effects on the environment that may result from the hazard (deposition maps identifying the potentially affected areas), and the vulnerability is expressed in terms of the environment susceptibility to transfer the radioactivity through the food chain pathway (vulnerability maps). This depends on the type of soil on which the radionuclides accumulate, and the type of crop grown in it, being the soil-to-plant transfer factor, the quantification parameter.

In the third stage of the **risk evaluation**, the results of the deposition and vulnerability analyses are **categorised** using a risk matrix with an indicator-based approach. The combination of the two final factors results in a **prioritisation** index, which maps the degree of priority of the potentially affected agricultural areas where recovery measures should be applied..

The following is a more detailed description of the various risk elements under consideration.

### **3.1 Hazard identification**

Hazard is any natural or man-made substance, chemical, physical or biological agent that can cause an adverse health outcome in certain circumstances. The identification and characterization of the hazards, i.e. a process of identifying and analysing sources of danger, is mandatory and the first step to deal with a risk assessment analysis.

The identification of hazards is not a simple matter, however. In many ways, it has become more difficult as the depth of technology has increased. On the other hand, a whole battery of hazard identification methods which may be used to solve these problems are now available.

A nuclear and radiological accident is defined by the IAEA as an event that has led to significant consequences for people, the environment or the facility (IAEA, 2016). The operation of nuclear facilities produces large quantities of radioactive material that can be released to the environment in airborne and liquid form. The hazard addressed in this report is the accidental release of radioactive material (source term) from nuclear facilities to the atmosphere and with potential off-site radiological consequences.

The source term is the timing and magnitude of a radioactive material release to the environment from a specific site. Under ANURE, source term information has been derived from existing studies providing a realistic evaluation of accident progression and offsite consequence releases from nuclear installations.

### **3.2 Estimation of effects and consequences of the release**

#### **3.2.1 Meteorological characterisation.**

Meteorological analysis is relevant for various applications related to the environment and provides an excellent description of the climate at the site. Meteorological conditions are one of the primary constraints on the geographic and seasonal distribution of pollutants (Fann et al., 2016) and infectious agents (Wu et al., 2016). More specifically, the potential release of radioactive materials to the atmosphere, undergo a process of atmospheric dispersion and deposition that is conditioned by factors such as wind speed and direction, and precipitation (Srinivas et al., 2012). Wind direction and speed determine the dispersion of the plume, while precipitation strongly influences the ground contamination. Therefore, variations in local weather conditions highly determine the atmospheric dispersal and deposition of radioactive material from the release point.

All meteorological analyses are primarily based on observations of the state of the atmosphere or weather. Meteorological observation plays a critical role in climatic study, and hence, the first-hand data for meteorology are provided by in situ measurements. The need to collect and store meteorological data is commonly accepted as important to the meteorological characterization in terms of statistical descriptions of the central tendencies and variability of relevant parameters such as precipitation and winds. The complete set of in-situ precipitation and wind data available are then analysed.

In general, the measured concentrations of air pollutants in the lower atmosphere are the result of the combined effect of several processes in the atmosphere, which may be divided into local, meso- and synoptic scale (Levy et al., 2010). Therefore, the dispersion pattern over a given region is driven from the large synoptic scale (length scale of the order of 1000 km or more) to the smaller mesoscale (hundreds of km) and down to the local scale (less than 1 km), and the interactions between them (e.g. Kalthoff et al., 2003).

Air trajectory analysis is a central scientific tool to characterize mesoscale wind regimes (e.g. Perez et al., 2015). When compiled and studied over multiple years (e.g. Toledano et al., 2009), the outcome of this trajectory analysis provides a reliable characterization of the wind patterns at the selected region, and, hence, it provides useful guidance in estimating the dispersion that might result if harmful material reaches the atmosphere. The basic methodological approach in this kind of analysis is to generate massive amount of air mass trajectories with the purpose to consider a large number of transport and dispersion scenarios, so that, the statistical analysis leads to extract representative information about wind patterns (e.g. residence time, number of patterns, origin and pathway, etc.).

The HYSPLIT model is used to compute the trajectories, i.e. the model computed air-mass locations (latitude, longitude and height above ground level) at one hour intervals (Stein et al., 2015). To compute the trajectories, the three hourly meteorological archive data from NCEP's GDAS (National Weather Service's National Centers for Environmental Prediction - Global Data Assimilation System) were used. These data are archived and made available by the NOAA's Air Resources Laboratory (ARL) as three hourly, global, one degree latitude longitude dataset on pressure surface (<sup>9</sup>).

### **3.2.2 Atmospheric dispersion simulation**

Radionuclides released into the atmosphere are transported with the mean wind, dispersed by turbulence and except for noble gas, deposited on the ground, either through precipitation (wet deposition) or/and just sticking to the surface (dry deposition). Estimation of the dispersion patterns and the potential levels of radioactive contamination can be achieved by using Atmospheric Dispersion Models (ADMs).

The basic methodological approach is to generate dispersion plumes for many possible meteorological conditions for a specific accidental release scenario defined by a given source term, so that these statistical results reflect the characteristics of the dispersion and deposition patterns for that source term. Therefore, this kind of work must involve large number of calculations with different meteorological scenarios.

The numerical dispersion calculations have been carried out using the JRODOS System (Realtime Online DecisiOn Support system) (KIT, 2017), for a defined accidental scenario, by means of the RIMPUFF atmospheric dispersion model, a Lagrangian atmospheric diffusion model developed by Risø DTU National Laboratory for Sustainable Energy, Denmark (Thykier-Nielsen et al., 1999), included in it. It is worth mentioning that the choice regarding, e.g. the grid size and time steps can influence results and certain parameters, and hence, uncertainties remain.

The model can cope well with the time-dependent and spatially inhomogeneous meteorological situations which are often of interest in connection with calculations used to estimate the consequences of the short-term (accidental) releases of airborne into atmosphere. The model applies both to homogeneous and inhomogeneous terrain with moderate topography and responds to changes in meteorological conditions. It can simulate the time changing releases of airborne materials by sequentially releasing a series of Gaussian shaped puffs at a fixed rate on a specified grid.

For calculation purposes, the meteorological data, which determine the temporal and spatial distribution of the plume, and the source term characteristics, which determine the timing and magnitude of the radioactive release to the environment from a specific source, are obtained as follows:

- The National Centers for Environmental Prediction/Global Forecast System analysis (NCEP-GFS) analysis data (GFS-ANL) available at the NOMADS website (<sup>10</sup>) with 0.5-degree resolution (Table 1). Due to continuous evolution and progress in the development of initial and boundary conditions, NCEP-GFS is currently the analysis dataset that are freely and publicly available and continue to be kept up to date. The possibility, both to get access to these meteorological files and to extent the analysis in the future from the base of the same meteorological inputs, were the major criteria for the selection of this dataset.
- The information regarding the source term has been obtained from existing studies, which provide a realistic evaluation of accident progression and off-site consequence releases from nuclear installations.

**Table 1.** Main characteristics of the NCEP-GFS dataset.

<b>Model</b>	<b>Period of record</b>	<b>Grid/scale</b>	<b>Model Cycle</b>	<b>Output Time step</b>
GFS Analysis (GFS-ANL)	01Jan2007–Present	004 (0.5°)	4/day: 00, 06, 12, 18UTC	+00, (+03, +06 precipitation fields)

Source: NOAA-NCEI, 2022 (<sup>11</sup>)

### **3.2.3 Deposition analysis**

Soil contamination levels can approach the severity of radiation exposure to the public and the environment due to deposition. They are primarily used to estimate potential doses to the population and, if this is the

(<sup>9</sup>) <https://www.ready.noaa.gov/gdas1.php>

(<sup>10</sup>) <https://nomads.ncep.noaa.gov/>.

(<sup>11</sup>) <https://www.ncei.noaa.gov/products/weather-climate-models/global-forecast>

case, to determine the need for decontamination. Action levels are usually established for specific radionuclides or their groups, such as,  $^{131}\text{I}$ ,  $^{90}\text{Sr}$  and  $^{137}\text{Cs}$  (IAEA, 2005). In the case of a nuclear accident, the decay of short-lived radionuclides and the consequent reduction of environmental radiation levels and activity concentrations should be considered. The objective of a recovery strategy and other actions to reduce the radiation dose is to obtain contamination levels as low as reasonably achievable (ALARA Principle).

For analysis purposes, the total deposition (dry and wet) predicted values of the radionuclides of concern at the end of the simulation, have been grouped into severity categories, in the absence of other references at European level, according to the contamination levels used as reference in the Nordic Guidelines and Recommendations 2014 (NGR, 2014) for strong gamma and beta emitters together, shown in Table 2. These are given by the Nordic radiation protection and nuclear safety authorities for protective measures in the early and intermediate phases of a nuclear or radiological emergency providing a common starting point for the practical application of protective measures for national authorities responsible for radiation protection in the event of a nuclear or radiological emergency.

**Table 2.** Contamination levels according to the activity concentration ( $\text{kBq m}^{-2}$ ) of strong gamma and beta emitters deposited on ground.

Contamination levels	Strong gamma and beta emitters ( $\text{kBq m}^{-2}$ )
Non-contaminated	No contamination at all or very low contamination
Slightly contaminated	< 100
Contaminated	100 - 1000
Heavily contaminated	1000 - 10000
Extremely contaminated	> 10000

Source: NGR, 2014.

### 3.3 Vulnerability assessment

The radiological vulnerability of the soil-plant-system is defined as the potential to transfer the activity concentration deposited on the soil to the population, through the food chain ingestion pathway. Therefore, the vulnerability depends on the type of soil on which the radionuclides accumulate, and the type of crop grown in it, being the soil-to-plant transfer factor, the quantification parameter.

The different behaviour of radionuclides in soils (e.g. Trueba, 2004 performed an analysis of  $^{137}\text{Cs}$  and  $^{90}\text{Sr}$  on Spanish soils), which vary according to the specific parameters that govern the retention and bioavailability processes, such as the soil texture, the cation exchange capacity and the K and Ca status, need to be considered. Regarding the crops, they do not have the same potential to incorporate radionuclides, showing differences in the root uptake process, e.g. green vegetables usually show the highest uptake values, whereas woody crops show the lowest (Nisbet and Woodward, 1998 and 2000). Therefore, the identification of different agricultural systems to apply the soil-to-plant transfer factors must be made by means of the soil and land use characterization that allow the soil type-crop association.

To assess the radiological vulnerability the following set of factors are taken into account: a) the soil type distribution (EC-ESBN, 2004) and topsoil properties (Trueba et al, 2015), which influence the radionuclide behaviour in soils, b) the land use (EEA, 2016), in order to assign where the different crops are grown in the affected area and c) the soil-to-plant transfer factors (IAEA, 2010), which quantify the crop root uptake processes and are specific for each soil texture-crop combination.

The methodology, that uses an indicator-based approach, is described in detail in García-Puerta (2020). The final output is a vulnerability map, made using GIS tools (ESRI, 2016), that categorises the transfer potential of the radionuclides deposited through the different soil-crop binomials.

### 3.4 Prioritisation maps

The large amount of dispersion simulations carried out, allows estimating the temporal and spatial variability of the affected area and the frequency of exceedance of contamination levels, i.e. deposition maps. This information, combined with detailed information of soil vulnerability and food chain impact, i.e. vulnerability maps, provides the spatial and temporal distribution of the prioritisation areas, and then, the risk associated with nuclear releases. These final maps can be used in the preparedness phase to determine the potential foodstuff and feedstuff restriction areas, or to establish where remediation and recovery measures could be applied.

## 4 Case study: Almaraz NPP

The Almaraz NPP (Lat = 39.80705, Long = -5.6986) has been selected as case study to train the methodology as a whole considering a reference period of five consecutive years (2012-2016).

The Power Plant is located in Almaraz de Tajo, in the Extremadura community, in the region of Campo Arañuelo (Cáceres) on a site bordered by the Tajo and Tiétar rivers. The land belonging to the plant occupies an area of 1,683 hectares, located in the Almaraz, Saucedilla, Serrejón and Romangordo municipalities. Of this, Almaraz NPP occupies an area of 428 hectares, excluding that flooded by the Arrocampo reservoir. The area used for Plant operations is approximately 1,123,000 m<sup>2</sup>, which incorporates the different industrial areas of the plant. The rest of the land is mostly mountainous terrain.

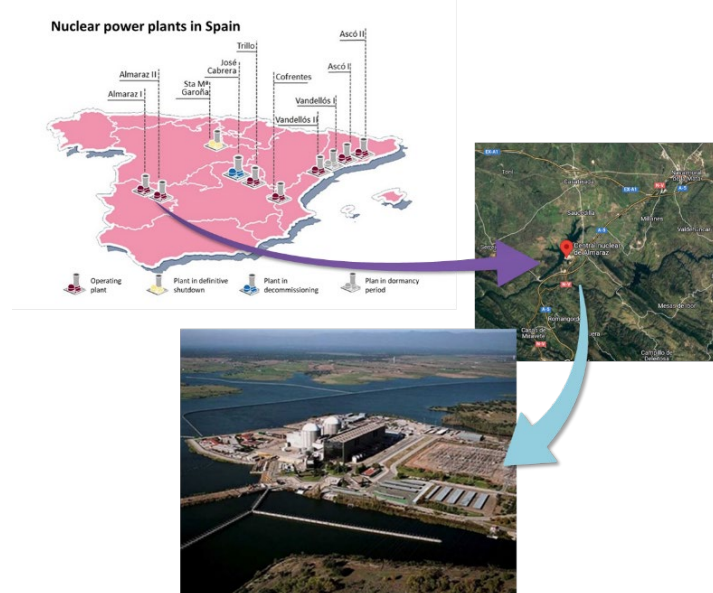
The climate in the area is continental, with low and erratic rainfall, making the environment an area with more pastures than crops, and pasture lands and irrigation are the two most common forms of land use. The proximity to large numbers of environmental protection areas is notable, including the Monfragüe National Park LIC (Site of Community Importance) and its ZEPA (Special Protection Area) and Environment Pastures alongside the Arrocampo (CNAT, 2019).

The selection of the Almaraz NPP was made due to the proximity to environmental protected areas as well as its proximity to the Portuguese border. The selection of a five-year period enables to work with a sufficiently large statistical sample, thus guaranteeing the representativeness of the different meteorological scenarios.

### 4.1 Almaraz NPP characteristics

The Almaraz NPP provides 16 billion kWh per year throughout Spain. It has two pressurized light water reactors (PWR), model Westinghouse 3-loop, of 2947 thermal power (MWt), each of them with three cooling circuits. They were brought into commercial operation in 1981 and 1984, respectively. Both units use as fuel slightly enriched uranium oxide, and their electric power is 1011 MWe and 1006 MWe respectively (CNAT, 2019). Almaraz NPP uses the Tajo River for cooling (Figure 2).

**Figure 2.** Almaraz NPP site.



Source: Own elaboration, CIEMAT, 2022, based on a graph from MITECO, 2022<sup>(12)</sup>, and photos from Google maps<sup>(13)</sup> (Terrametrics, 2022) and EFE/lafototeca.com, 2010<sup>(14)</sup>, respectively.

<sup>(12)</sup> <https://energia.gob.es/nuclear/Centrales/Espana/Paginas/CentralesEspana.aspx>

<sup>(13)</sup> <https://www.google.es/maps/place/Central+nuclear+de+Almaraz/>

<sup>(14)</sup> TAG ID: efespfive670049. <http://www.lafototeca.com/>

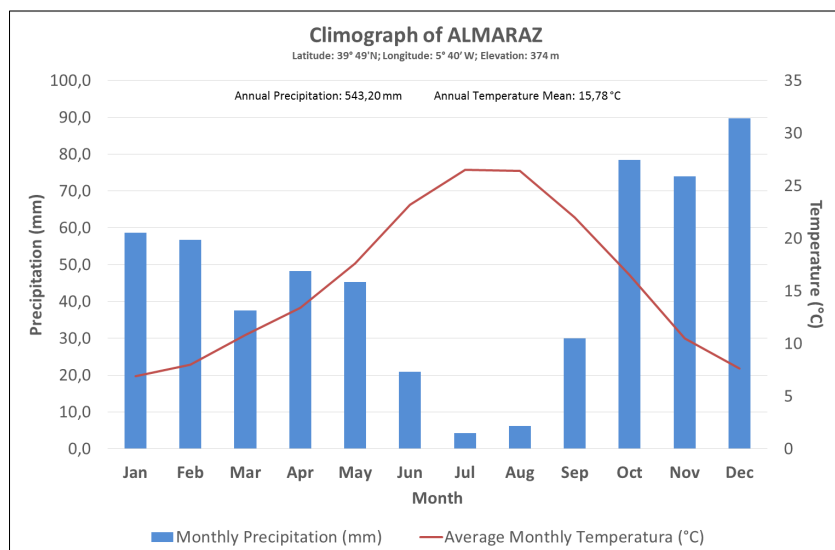
## 4.2 Meteorological characterisation

### 4.2.1 Local-scale wind and precipitation patterns

Almaraz NPP employs meteorological stations to continuously measure and record the most significant meteorological parameters such as temperature, precipitation, wind direction and speed, humidity and solar radiation. The following analysis focused on the wind speed and direction, and the precipitation are based on data measured "in situ" by weather stations at the Almaraz NPP from 1972 to 2009.

Figure 3 shows the annual and monthly evolution of the total precipitation during this period. Yearly changes are apparent, with a maximum above 900 l m<sup>-2</sup> in 1997 and a minimum of 260 l m<sup>-2</sup> in 1984. In the same line, the seasonal variability is substantial. This figure displays the strong seasonal variation of the precipitation in this area, decreasing from autumn (October, November and December) to summer (June, July, August). The monthly average precipitation of December and July reflects the major difference for precipitation between months.

**Figure 3.** Climograph of Almaraz site, Cáceres (Spain), 1972 to 2021.

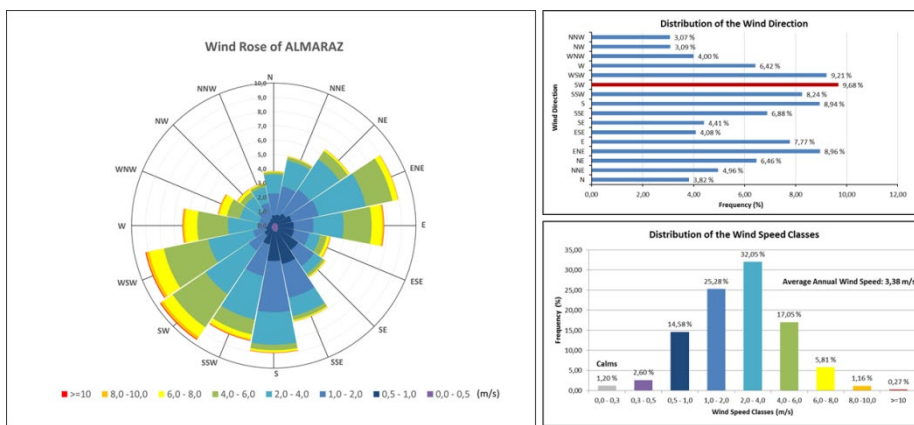


Source: Own elaboration, CIEMAT 2022. Temperature Data: (1991-2021), Climate-Data.org<sup>(15)</sup>. Precipitation Data: (1972-2009), from Meteorological dataset used in the Almaraz NPP Safety Study, CSN, 2013 (personal communication).

Regarding the local wind speed and direction, Figure 4 shows the wind speed and direction distributions at Almaraz NPP for the period 1972-2009. This figure shows how this site is normally affected by airflows from the northeast-east, and southwest-west, while the arrival of northerly airflows is less frequent. Almaraz NPP is placed at the end of the Arrocampo reservoir in the Tajo river valley, which broadens to the East and narrows to the West, while being flanked by mountains with heights up to 1000 m above sea level (a.s.l.) in the North and the South. By its location, a channelling of the dispersed plume through the valley is often expected in case of an accidental release during strong wind situations. Wind speeds at Almaraz NPP are mainly below 10 m s<sup>-1</sup>, and there is a large frequency of calms (< 1 m s<sup>-1</sup>).

(15) <https://es.climate-data.org/europe/espana/extremadura/almaraz-412069/#climate-graph>

**Figure 4.** Characteristic wind rose for the Almaraz NPP site including the distribution of the frequencies of wind speed and wind direction.



Source: Own elaboration, CIEMAT 2022. Wind data (1972 -2009) from Meteorological dataset used in the Almaraz NPP Safety Study, CSN, 2013 (personal communication).

#### 4.2.2 Regional-scale wind patterns

To this purpose, an air mass trajectory analysis was carried out. Forward daily kinematic three-dimensional trajectories with duration of 120 hours were calculated by using the HYSPLIT model (Stein et al., 2015) for the 2012-2016 period. The model computed air-mass locations (latitude, longitude and height above ground level) in intervals of 1 hour, i.e. trajectory endpoints. The methodology used to represent this large amount of information is detailed in Annex 1. It is based on the calculation of density maps from the set of air mass trajectories for a period of 5 years (2012-2016) by applying the kernel density estimation method (Shi, 2010). This method creates a smoothed density surface based in which the values read from the map may not match the total percentage of trajectory endpoints within a specific grid cell. The label of the density map obtained refers to high or low density of points. In this present framework, these density maps report both the dispersion patterns from the Almaraz NPP and the areas with the longest residence time of air masses, and hence, the areas where the deposition maybe substantial.

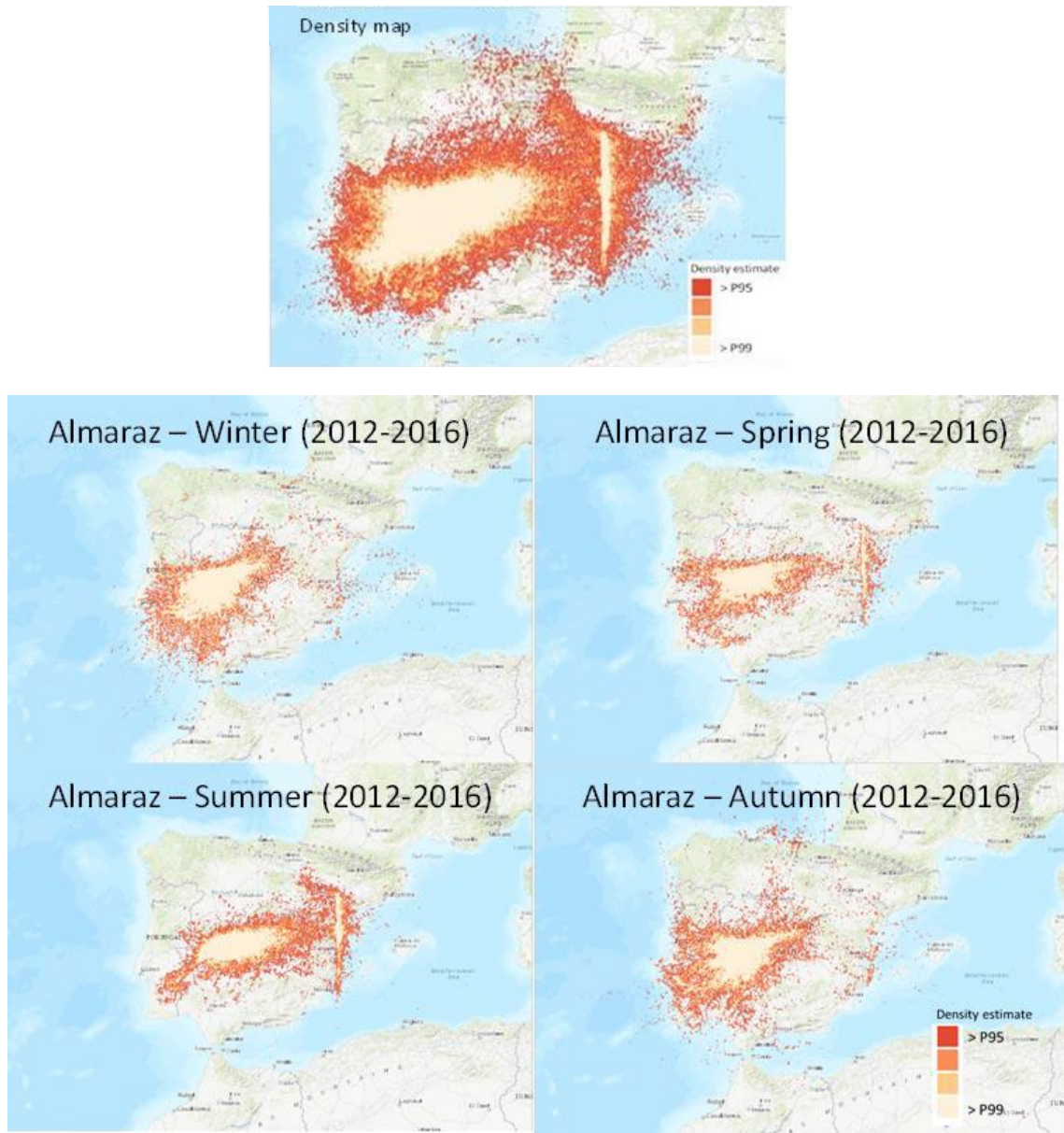
Figure 5 shows the density map for the 2012-2016, period at Almaraz NPP. The maps only show those grid cells with a density value above the 95th Percentile. This figure shows a main airflow pattern along the Northeast - Southwest axis. This dispersion pattern agrees with the most frequent wind directions shown in Figure 4.

In a broader view, the shape of the density map is also in agreement with the barrier effect created by the mountains surrounding the Iberian Plateau, a vast plateau in the heart of the Iberian Peninsula with an elevation that ranges from 610 to 760 m. The mountain regions surrounding the Iberian Plateau are the Sierra Morena to the South, the Cordillera Cantábrica to the North and the Sistema Ibérico to the Northeast. In this case, it is also possible to identify the impact of the Pyrenees. This map also shows high density values along the Mediterranean coast (from the North to the South), which can be associated with the blocking effect of the winds arriving from the West. However, this high-density area also coincides with the Greenwich meridian, which is used to indicate 0° Longitude and hence, the “start” of West and East. Due to this coincidence, further analysis is needed to clarify the potential impact of this fact on the results.

Figure 5 also shows the seasonal variation of the dispersion pattern considering the 2012-2016 period. This seasonal airflow pattern provides evidence of different air mass movements along the year, and hence, the spatial and temporal variability of the areas potentially affected by the passage of contaminated air masses. Wind direction is mainly to the Southwest in winter, while it becomes more variable in spring, between Southwest and East. In contrast, wind direction is mainly to the East in summer, while this component reduces in autumn, when there is a similar pattern in winter. These changes reflect the annual cycle of the synoptic circulation patterns affecting the Iberian Peninsula, and how summer and winter can be allocated in the extremes while spring and autumn can be considered as transition periods.

Additionally, a methodology to characterize the atmospheric transport and dispersion tendencies in a particular site, based on the prevalent airflow patterns was developed and is explained in Annex 2 (Hernández-Ceballos et al., 2020).

**Figure 5.** Density map for the period 2012-2016, as well as the corresponding seasonal density maps for the same period, i.e. Winter (from 22<sup>nd</sup> December to 21<sup>st</sup> March), Spring (from 22<sup>nd</sup> March to 21<sup>st</sup> June), Summer (from 22<sup>nd</sup> June to 21<sup>st</sup> September) and Autumn (from 22<sup>nd</sup> September to 21<sup>st</sup> December).



Source: Own elaboration. JRC, 2017

### 4.3 Estimation of effects and consequences of the release

#### 4.3.1 Atmospheric dispersion simulations

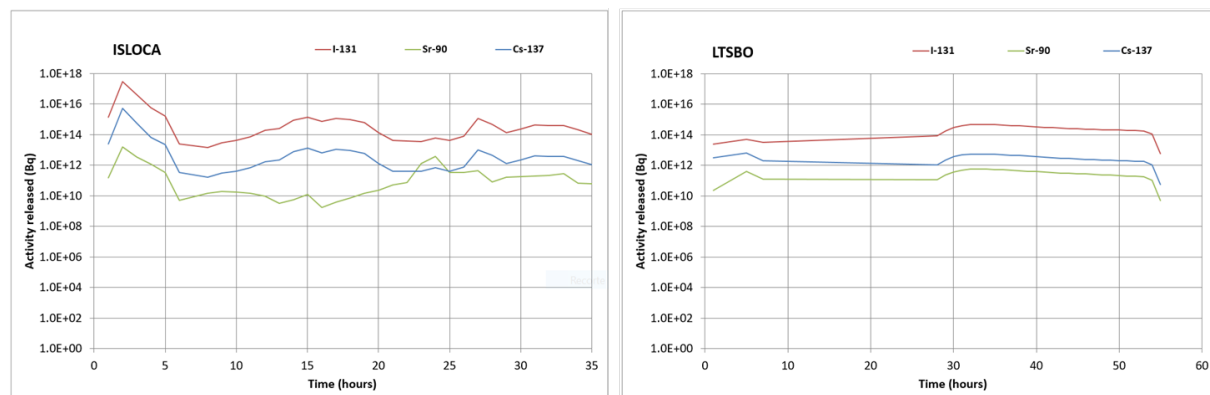
Regarding the source term, information has been derived from existing studies providing a realistic evaluation of accident progression and off-site releases from nuclear installations. Considering the characteristics of the Almaraz NPP, the integrated analysis on the Surry NPP (Virginia, USA) (USNRC, 2012), within the State-of-the-Art Reactor Consequence Analyses (SOARCA) Project, has been chosen as surrogate for source term estimation purposes.

It is important to note that the use of the Surry source term for Almaraz is still a theoretical exercise, and the results cannot be used in applications that require an accurate analysis of the specific characteristics of the plant, such as the Probabilistic Safety Analysis (PSA). However, in the present study, in which the target is to train a methodology to assess the off-site radiological consequences of severe NPP accidents considering the varying meteorological conditions, the analysis does not lose validity.

SOARCA considers 1) accident sequences with estimated frequencies above  $1.0 \text{ E}^{-6}$  per reactor and year as candidate for further deterministic evaluation, and 2) accident sequences below  $1.0 \text{ E}^{-6}$  per reactor and year are judged to proceed rapidly enough to have the potential for generating significant early releases of radionuclides to the environment. Within this frame, two accidents have been chosen for the analysis of a release with potential off-site radiological consequences: *i*) an interfacing system loss-of-coolant accident (ISLOCA), initiated by an internal event caused by an unisolated rupture of low-head safety injection piping outside containment, with 35 hours of offsite radionuclide release and, *ii*) a long-term station blackout (LTSBO), initiated by an external event resulting in loss of offsite and outside AC power, with 55 hours of release.

A source term reduced to the radionuclides  $^{131}\text{I}$ ,  $^{137}\text{Cs}$  and  $^{90}\text{Sr}$  has been considered for purposes of the case study. Therefore, the source terms for Almaraz have been obtained applying the given release fractions for the halogens, alkaline earths and alkali metals classes for both accident sequences (USNRC, 2012), grouped on an hourly basis, to the respective inventory of  $^{131}\text{I}$ ,  $^{90}\text{Sr}$  and  $^{137}\text{Cs}$  of the Almaraz NPP included in the JRODOS Database.. The estimations of the activity released of these radionuclides during both sequence accidents are shown in Figure 6. Additional information on the process following to estimate these values is shown in Annex 3.

**Figure 6.** Estimation of the activity of  $^{131}\text{I}$ ,  $^{90}\text{Sr}$  and  $^{137}\text{Cs}$  released in time (hourly basis) for the ISLOCA (left-hand side) and LTSBO (right-hand side) sequence accidents.



Source: Own elaboration. CIEMAT, 2022.

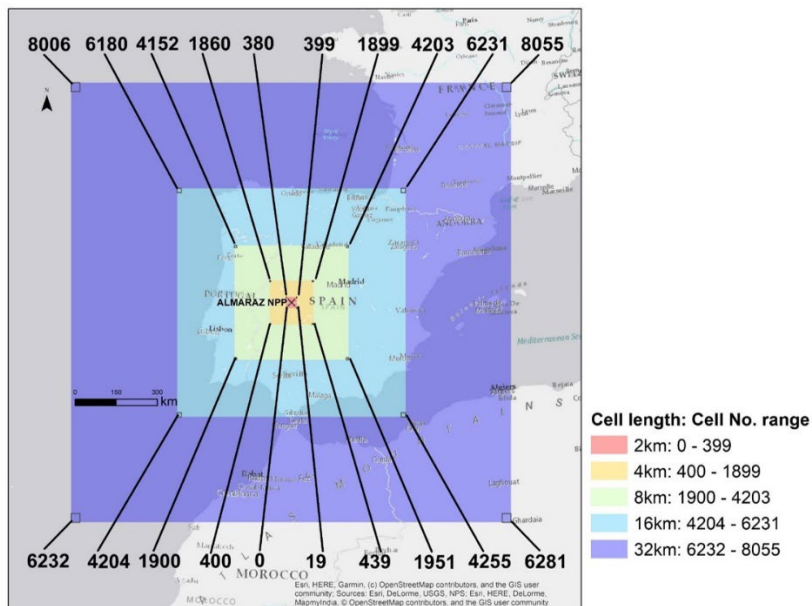
Daily releases, its dispersion and deposition were independently simulated for a five-year period (2012-2016) by the Lagrangian mesoscale atmospheric dispersion puff model RIMPUFF of JRODOS System for each type of accident. The Global Forecast System (GFS), which is a weather forecast model managed by the NCEP, has been used as meteorological input. Annex 4 describes briefly the meteorological input.

In order to ensure that the total release of these three radionuclides is fully deposited, a prognosis time of 48 hours is added in the calculations after finishing each release. Each ISLOCA accident simulation was therefore performed for 83 hours (35 hours of release and 48 hours of prognosis period). Similarly, the simulations conducted for a LTSBO accident result in 103 hours. Annex 5 contains the description of the RIMPUFF ADM and an Emergency Lite simulation using JRODOS. Due to gaps in the meteorological files and/or missing files, the number of simulations covering the whole simulation period is 76% out of the 1825 possible ones along the five-year period (1383 simulations), which is still a sufficient number to obtain illustrative results. The results of the simulations, as data tables on a excel sheets have been stored in the JRC repository<sup>16</sup> and can be reused for further analyses.

Ground contamination of  $^{131}\text{I}$ ,  $^{90}\text{Sr}$  and  $^{137}\text{Cs}$  are estimated at cell level on a non-homogeneous geographical grid spacing which comprise the study area. The chosen radius of calculation was 800 km, which corresponds to a minimum grid cell size of 2 km around the point of release (up to 50 km), 4 km up to 100 km, 8 km up to 200 km, 16 km up to 400 km and 32 km up to 800 km. The fine grid cell size of 2 and 4 km is appropriate to resolve with high resolution the plume dispersion and deposition at source distance up to 100 km, with the requirements of ANURE. Figure 7 shows the grids used.

<sup>(16)</sup> <https://data.jrc.ec.europa.eu/collection/id-00336>

**Figure 7.** Numerical grid for calculation used in the Almaraz case study. Projection: UTM WGS84 Zone 33.

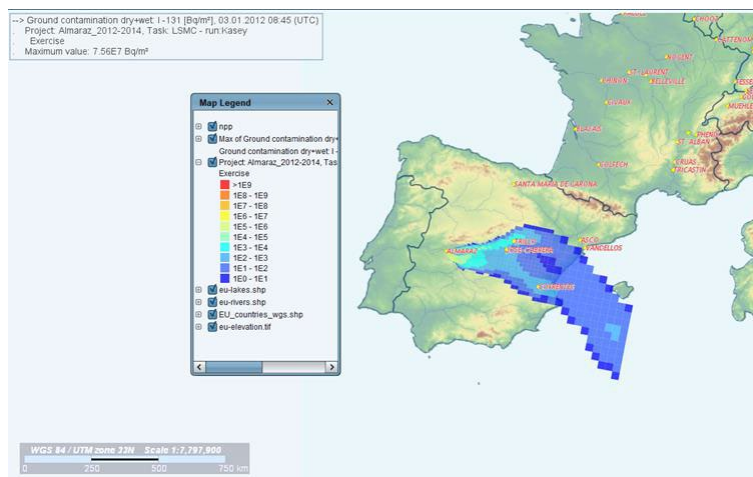


Source: García-Puerta, B., 2020

As an example of the model prediction used in this analysis, Figure 8 shows the ground deposition of  $^{131}\text{I}$  following an ISLOCA source term release (in  $\text{Bq m}^{-2}$ ) over the simulation spatial domain.

Due to the large number of modelling results obtained, a procedure to extract, store and make available this amount of information was designed. The procedure is explained in Annex 6. From this kind of model simulation results, various post-processing tasks were also carried out to achieve the project's goals. Examples of this post-processing are also included in Annex 6.

**Figure 8.** Example of the  $^{131}\text{I}$  deposition [ $\text{Bq m}^{-2}$ ]. Projection: UTM WGS84 Zone 33.

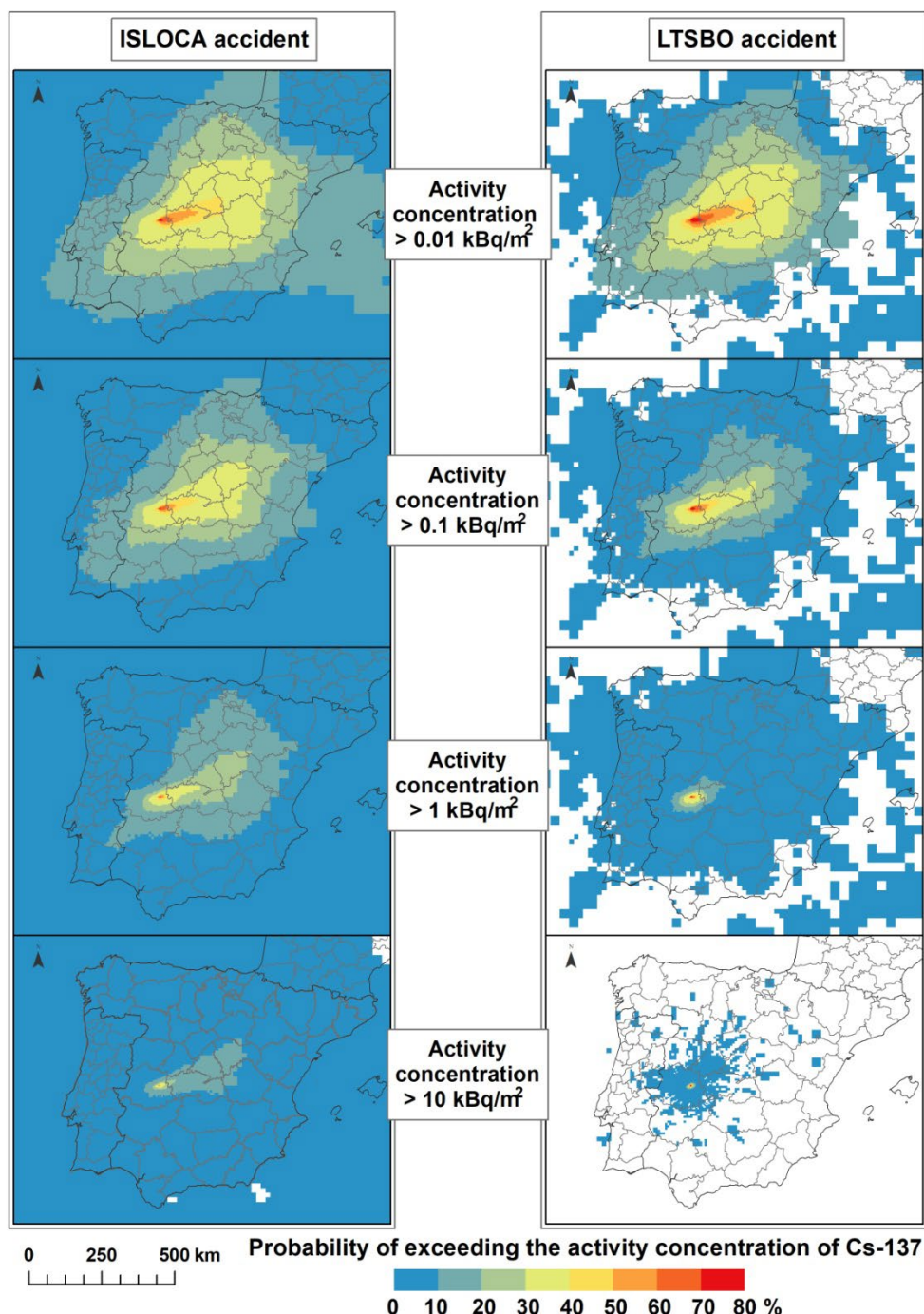


Source. Own elaboration. JRODOS software display, 2018.

Considering the results obtained from the whole bunch of simulations for each type of accident (ISLOCA or LTSBO), a probability analysis regarding the activity concentration deposited on the ground was developed. This task was performed in the frame of the Master Thesis of Garcia-Puerta, 2020. Four activity concentration ranges of  $^{137}\text{Cs}$  are taken into account for that purpose: over  $0.01 \text{ kBq m}^{-2}$ , over  $0.1 \text{ kBq m}^{-2}$ , over  $1.0 \text{ kBq m}^{-2}$ , and over  $10.0 \text{ kBq m}^{-2}$ . In Figure 9, the resulting deposition probability maps are shown. It can be noted that the ISLOCA accidental scenario would affect a larger area than the LTSBO for every deposition ranges and the

likelihood of having non-impacted grid cells in the former is limited. Therefore, the ISLOCA accident was the one considered to set the case study in order to study the risk posed by an accidental release from the selected site.

**Figure 9.** Probability analysis of the  $^{137}\text{Cs}$  deposited considering the simulations performed for an ISLOCA (left-hand side) and a LTSBO (right-hand side) accident scenarios in Almaraz NPP. The ranges of activity concentration deposited on ground are, from top to bottom, over  $0.01 \text{ kBq m}^{-2}$ , over  $0.1 \text{ kBq m}^{-2}$ , over  $1.0 \text{ kBq m}^{-2}$  and over  $10.0 \text{ kBq m}^{-2}$ .  
Projection: UTM ETRS89 Zone 30.



Source: Own elaboration. García-Puerta, 2020.

The probability of occurrence of depositions and the probability of occurrence of depositions above a fixed activity concentration value, e.g. threshold of protective measures, at every grid cell also can be mapped for each one of the airflow patterns, as shown in Annex 2.

### 4.3.2 Deposition maps

The total deposition (dry and wet) values of  $^{131}\text{I}$ ,  $^{90}\text{Sr}$  and  $^{137}\text{Cs}$  predicted at each grid cell at the end of each simulation (83<sup>rd</sup> hour), have been grouped into the contamination levels shown in Table 2.

These refer to the external dose rate ( $\mu\text{Sv h}^{-1}$ ) and the activity concentration deposited on soil from alpha emitters and strong beta and gamma emitters ( $\text{kBq m}^{-2}$ ). For ANURE purposes, and with the aim of showing the implementation of the methodology proposed, only the results for  $^{137}\text{Cs}$  are displayed. It is important to outline that the contribution of this radionuclide to the ground contamination, among all the deposited radionuclides, has been estimated at  $10^{-3}$  times with respect to the total activity concentration deposited. The activity concentration deposition thresholds, given in  $\text{kBq m}^{-2}$  for those emitters have been adjusted taken into consideration exclusively the  $^{137}\text{Cs}$  contribution, as shown in Table 3. With the aim to distinguish the cases where the grid cells have not been impacted with any deposition, a new contamination level has been added to the five initial ones, named "Non-impacted".

In order to identify the potentially affected areas by the deposition occasioned by the accidental release, a *Deposition Index* is defined in terms of probability of occurrence and contamination level to map the deposition pattern obtained from the whole set of simulations done. A *Deposition Weighting Factor* is defined to weight the contribution of each possible contamination level encountered in the grid cells impacted among all the simulations done. Different values of the *Deposition Weighting Factor* are associated to the different contamination levels, as shown also in Table 3, in which it is also included the threshold related to the corresponding contribution of  $^{137}\text{Cs}$ . For the same probability of occurrence of different contamination levels, the higher is the *Deposition Weighting Factor*, the higher is the *Deposition Index*.

**Table 3.** Contamination levels considered in ANURE, with their corresponding activity concentration ranges of the total of strong gamma and beta emitters deposited on ground and the corresponding contribution of  $^{137}\text{Cs}$ , and the Deposition Weighting Factors associated.

Contamination level <sup>(1)</sup>	Activity concentration deposited ( $\text{kBq}\cdot\text{m}^{-2}$ )	$^{137}\text{Cs}$ Activity concentration deposited ( $\text{kBq}\cdot\text{m}^{-2}$ )	Deposition Weighting Factor
Non-impacted	0	0	1
Non-contaminated	0-10	0-0.01	$1\cdot10^1$
Slightly contaminated	10-100	0.01-0.1	$1\cdot10^2$
Contaminated	100-1000	0.1-1.0	$1\cdot10^3$
Heavily contaminated	1000-10000	1.0-10.0	$1\cdot10^4$
Extremely contaminated	>10000	>10.0	$1\cdot10^5$

<sup>(1)</sup> NGR, 2014 define the lower contaminated category as "Non-contaminated" for activity concentration levels under  $100 \text{ kBq}\cdot\text{m}^{-2}$ . That classification was adapted for methodological purposes to include a lower threshold of  $10 \text{ kBq}\cdot\text{m}^{-2}$  in the "Slightly contaminated" category, as well as another contamination level, "Non-impacted", to distinguish those cases where there is no deposition at all, from the cases affected with the considered lower activity concentration.

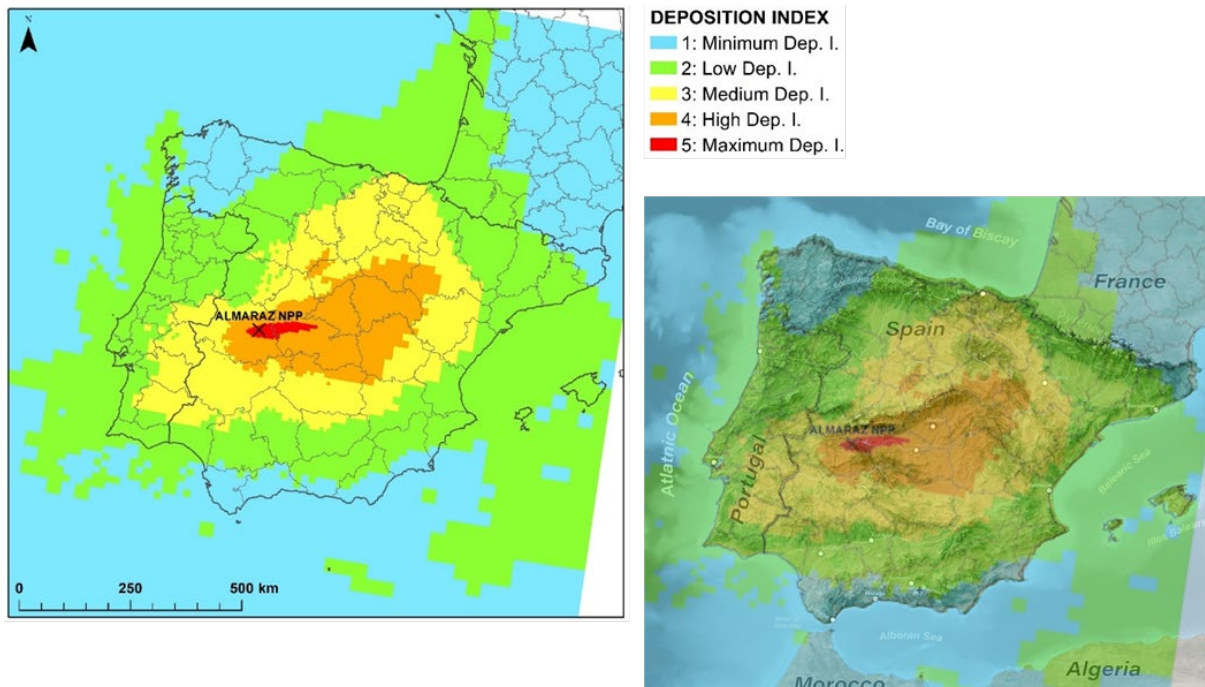
Source: Own elaboration, from contamination levels in NGR, 2014. CIEMAT, 2020.

For each grid cell, every deposition value obtained in each simulation is classified according to the categories defined in Table 3. The probability of occurrence of each contamination level is assessed and multiplied by its corresponding *Deposition Weighting Factor* (see Table 3); then, all the products are summed. The result is an indicator of the predominant average deposition estimated for each cell in the scenario representative for the release of the ISLOCA accident. The sums in all grid cells are considered to assess the corresponding percentiles: 25, 50, 75 and 95, which are used as thresholds to elaborate the *Deposition Index*. This new index is distributed in five classes ranging from 1 (for sum values under the percentile 25), representing the minimum deposition, in terms of both probability of occurrence and activity concentration magnitude, to 5 (for sum values over the percentile 95), which represent the maximum deposition.

In Figure 10, the spatial distribution of this deposition index is shown. As seen, the estimated deposition pattern follows a South West-North East axis, in agreement with the shape of the density map showed previously and the dominant wind direction. The entire Iberian Peninsula would be affected but with different degree of deposition severity, which is largely determined by the Iberian Peninsula relief (the Central Plateau, and mountains systems surrounding and outside it, and depressions). According to this pattern, the surroundings of the Almaraz NPP show the maximum deposition index, extending beyond the regional level,

more than 150 km away from the site. The high deposition index occupies nearly all the province of Cáceres and spreads beyond the centre of the Peninsula, around 600 km away from the NPP site. The medium deposition index follows the same pattern than the previous one but occupies a larger surface, affecting also Portugal.

**Figure 10.** Annual  $^{137}\text{Cs}$  Deposition index average map (on the left) along 2012-2016 period (Projection: UTM WGS84 Zone 33); on the right, the map has been superimposed over an image of the Iberian Peninsula relief, showing the influence of the relief on the zoning.



Source: Own elaboration, CIEMAT, 2022. Map of Iberian relief from scaredortolan, 2021 (17)

The map shown refers to the average annual meteorological conditions, but more accurate maps can be obtained for each season of the year, by analysing separately the simulations corresponding to each one of them.

#### 4.4 Vulnerability Assessment

To assess the radiological vulnerability, the following set of factors are taken into account: *a*) the soil type distribution (EC-ESBN, 2004) and topsoil properties (Trueba et al, 2015), which influence the radionuclide behaviour in soils, *b*) the land use (EEA, 2016), in order to assign where the different crops are grown in the affected area and *c*) the soil-to-plant transfer factors (IAEA, 2010), which quantify the crop root uptake processes and are specific for each soil texture-crop combination. In this case study, rainfed cereals are the crops considered to establish the radiological vulnerability of the soil-plant system, because of their wide distribution.

The  $^{137}\text{Cs}$  transfer from soil to plant is highly influenced by the K status and the clay content in soils. Potassium is a basic nutrient for plants and radiocaesium competes with it in the root uptake process, due to their similar physicochemical properties. On the other hand, clay has the capacity to retain K at different degrees according to the clay type and therefore, in a more or less exchangeable way, clay acts as reservoir of K, but also of Cs if it were present in the soil. It can be assumed that the higher the K status and clay content in soils, the more saturated it is in K and lower in bioavailable  $^{137}\text{Cs}$  content in the soil solution. To define the soil capability for having available  $^{137}\text{Cs}$  for crop root uptake, a qualitative index has been defined relating the soil K reservoir with the bioavailable K status depending on the clay topsoil content as seen in Table 4 (Domínguez Vivancos, 1997). This index is called *Caesium Bioavailability Index (I\_Cs)*, and ranges from 1 (for the lowest caesium bioavailability) to 5 (for the highest caesium bioavailability).

(17) [https://www.reddit.com/r/gis/comments/mh4vl2/map\\_of\\_the\\_iberian\\_peninsula/?utm\\_source=share&utm\\_medium=web2x&context=3](https://www.reddit.com/r/gis/comments/mh4vl2/map_of_the_iberian_peninsula/?utm_source=share&utm_medium=web2x&context=3)

**Table 4.** Caesium Bioavailability Index ( $I_{Cs}$ ) definition, considering clay and K soil content.

Caesium Bioavailability Index	Potassium Reservoir in Soil	Bioavailable K content in Soil (cmol·kg <sup>-1</sup> ) depending on clay content			
		$I_K$	Clay 0-10 %	Clay >10-20 %	Clay >20-30 %
$I_{Cs}$					
1	Very High		>0.5	>0.8	>0.9
2	High		>0.4-0.5	>0.6-0.8	>0.7-0.9
3	Medium		>0.2-0.4	>0.5-0.6	>0.6-0.7
4	Low		>0.1-0.2	>0.3-0.5	>0.4-0.6
5	Very Low		<=0.1	<=0.3	<=0.4
					<=0.5

Source: Domínguez Vivancos, 1997.

The  $I_{Cs}$  is assessed by using the soil type distribution proposed in (Trueba, 2004 and Trueba and Vallés, 2000) and considering K and clay topsoil content, obtained from the Spanish soil profile database (Trueba et al, 2015). The  $I_{Cs}$  is mapped by assigning the assessed index value to each Soil Mapping Unit (SMU) – which corresponds to each soil association (EC-ESBN, 2004) –, according to its soil properties.

As said before, the quantification of the crop root uptake processes is made by means of the soil-to-crop transfer factor (TF). It is important to highlight that, for the same radionuclide, different groups of crops show different affinities for its uptake and that, in addition, among the crops belonging for the same group, there are also differences according to the type of soil in which they grow (IAEA, 2010), therefore transfer factors, are specific for each soil-crop combination. In this case, the soil parameter that defines the type of soil is its texture.

To introduce this quantification into the methodology, a *Soil-to-Crop Transfer Index* ( $I_{TF}$ ) has been defined, ranked from the lowest to the highest mean transfer factor value for the main mineral topsoil textures<sup>18</sup>. Empirical values of the <sup>137</sup>Cs transfer factors for cereals (IAEA, 2010) and the corresponding  $I_{TF}$  indexes, are shown in Table 5.

**Table 5.** Transfer factor values for grain cereals in temperate environments and the respective Soil-to-Crop Transfer Index assigned as function of the soil texture.

Texture	Sample number	Mean	Standard deviation	Minimum	Maximum	Soil-to-Crop Transfer Index ( $I_{TF}$ )
Sand	156	$3.90 \times 10^{-2}$	3.3	$2.00 \times 10^{-3}$	$6.60 \times 10^{-1}$	3: High
Loam	158	$2.00 \times 10^{-2}$	4.1	$8.00 \times 10^{-4}$	$2.00 \times 10^{-1}$	2: Medium
Clay	110	$1.10 \times 10^{-2}$	2.7	$2.00 \times 10^{-4}$	$9.00 \times 10^{-2}$	1: Minimum

Source: Modified from IAEA, 2010.

The  $I_{TF}$  is also assessed according to the soil type distribution and the soil texture (Trueba et al, 2015) and in those areas where rainfed cereals can be grown, it can be mapped.

A matrix to combine the *Caesium Bioavailability Index* ( $I_{Cs}$ ) and the *Soil-to-Crop Transfer Index* ( $I_{TF}$ ) is used. The combination is made by multiplying both indexes. In Figure 11 all the possible combinations among them are shown. The resultant values are grouped and reclassified into five categories to obtain the *Radiological Vulnerability Index* (see Figure 11).

<sup>18</sup> Organic soils are not considered because of their very low representativeness in the Iberian Peninsula.

**Figure 11.** Matrix to define the *Radiological Vulnerability Index* and definitive values for this index: from 1 to 5.

Combination matrix to obtain the *Radiological Vulnerability Index*:

TF Index		Min. TF	Low TF	High TF
Cs-137 Bioavailability Index	1	2	3	
	Very Low Bioavailability	1	2	3
	Low Bioavailability	2	4	6
	Medium Bioavailability	3	6	9
	High Bioavailability	4	8	12
Very High Bioavailability	5	10	15	

*Radiological Vulnerability Index* values:

1	1: Minimum Vulnerability
2 - 3	2: Low Vulnerability
4 - 6	3: Medium Vulnerability
8 - 12	4: High Vulnerability
15	5: Maximum Vulnerability

Source: Own elaboration, CIEMAT, 2019.

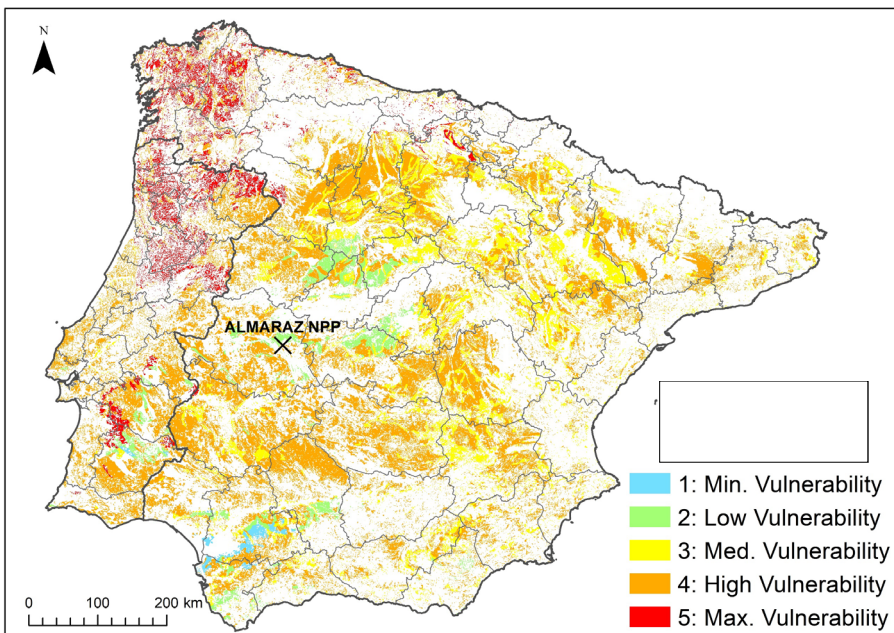
The elaboration of the Radiological Vulnerability map is done by using (ESRI, 2016): overlapping the map representing the *Caesium Bioavailability Index* and the *Soil-to-Crop Transfer Index* map. This way, independent cartographic units, with different combination of both indexes, can be separated. Then, the multiplication between both indexes in each cartographic unit is done and the reclassification of the resultant values, following the criteria shown in Figure 11, is made.

In this case, in addition to the soil properties, it is necessary to take into consideration the crop distribution in the IP. Corine Land Cover (EEA, 2016) is used to do so identifying the areas where the rainfed cereals grow in the agricultural areas which correspond to the following land uses:

- Non-irrigated arable land (land use code 211).
- Annual crops associated with permanent crops (land use code 241).
- Complex cultivation patterns (land use code 242).
- Land principally occupied by agriculture (land use code 243).
- Agro-forestry areas (land use code 244).

Once having selected those areas, every spot can be characterised according to its soil properties and crop, and thus the *Radiological Vulnerability Index* can be assessed and mapped, helping to identify visually the most radiologically vulnerable areas. As shown in Figure 12, the maximum *Radiological Vulnerability* indexes of the rainfed cereals to a  $^{137}\text{Cs}$  deposit, correspond to those areas where the higher TF values and the higher radiocesium bioavailability conditions (due to the small potassium reservoir in soils) concur. This situation stands out basically in the West of the Iberian Peninsula, characterized by having an acidic bedrock. The high vulnerability indexes are the most widely spread. They correspond to those areas in which high TF values coincide with high to medium radiocesium bioavailability conditions, and low TF values concur with maximum to high radiocesium bioavailability. Medium vulnerability indexes are not so extended as the previous one, being the low and minimum vulnerability indexes spotted at certain areas. The Almaraz NPP site is located in one of these spots where medium to low  $^{137}\text{Cs}$  bioavailability concur with high to low TF values.

**Figure 12.** Radiological Vulnerability map. Projection: UTM WGS84 Zone 33.



Source: Own elaboration, CIEMAT, 2019.

#### 4.5 Identification of prioritisation areas: nuclear risk maps

Considering both defined indexes: *Deposition Index* and *Radiological Vulnerability Index*, the agricultural areas where to act on, in case a nuclear accident occurs, are identified and classified in order to prioritise those where recovery actions are to be taken first, mainly focussed on the reduction of the  $^{137}\text{Cs}$  transfer from soil to cereals facing the subsequent growing seasons.

The *Prioritisation Index* is obtained by multiplying the *Deposition Index* and the *Radiological Vulnerability Index* using, again a matrix in which all the possible combinations are reflected (Figure 13). A categorisation of the outcomes from that multiplication is made to attain a ranking of the priority affected area to act on. The resultant Prioritisation map is performed by using (ESRI, 2016): overlapping the Deposition map and the Radiological Vulnerability map for rainfed cereals in a way that cartographic units are attained for different pair indexes values. Thus, having both indexes values for each spot, the multiplication between them is done to define the *Prioritisation Index*.

**Figure 13.** Matrix to define the Prioritisation of the agricultural contaminated areas facing their long-term recovery, by combining the *Deposition Index* and the *Radiological Vulnerability Index*.

Combination matrix to obtain the *Prioritisation Index*:

Rad. Vulnerability Index		Min. R.V.	Low R.V.	Med. R.V.	High R.V.	Max. R.V.
Deposition Index		1	2	3	4	5
Minimum Dep. I.	1	1	2	3	4	5
Low Dep. I.	2	2	4	6	8	10
Medium Dep. I.	3	3	6	9	12	15
High Dep. I.	4	4	8	12	16	20
Maximum Dep. I.	5	5	10	15	20	25

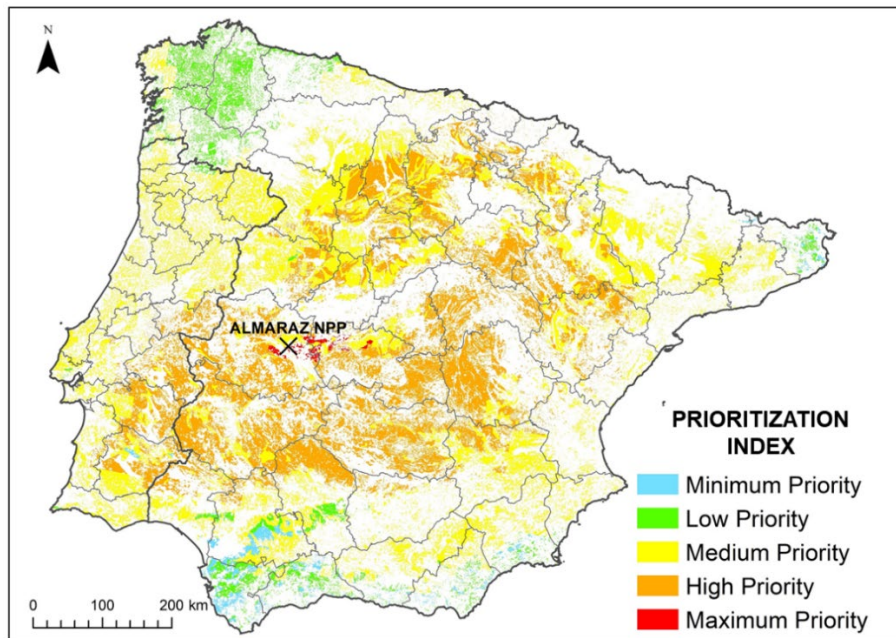
Prioritisation Index values:

1 - 3	Minimum Priority
3 - 5	Low Priority
6 - 10	Medium Priority
12 - 16	High Priority
20 - 25	Very High Priority

Source: Own elaboration, CIEMAT, 2019.

Figure 14 shows the spatial distribution of this *Prioritisation Index*. This map raises the overall risk categorisation and allows identifying and classifying the areas where the recovery actions are to be undertaken first.

**Figure 14.** Prioritisation map for cereals and  $^{137}\text{Cs}$  deposition. Projection: UTM WGS84 Zone 33.



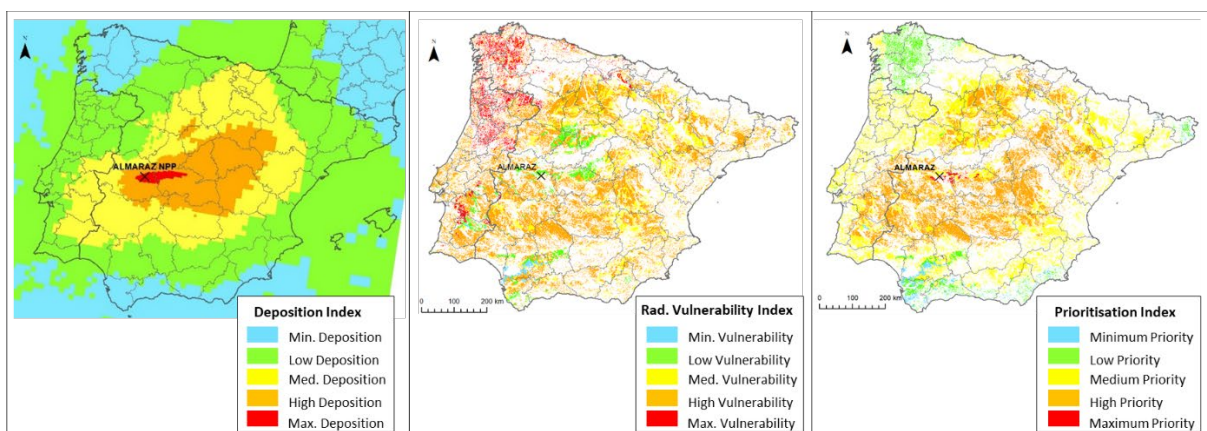
Source: Own elaboration, CIEMAT, 2019.

The maximum priority indexes, that is, where the recovery actions should be taken firstly, are located in scattered spots in the vicinity of Almaraz NPP and along an East-West axis within the area affected with the maximum deposition index (following the Tajo basin). The first remediation actions should be applied there, with the aim of reducing the  $^{137}\text{Cs}$  root uptake for the next year harvested cereals.

Figure 14 shows a wide display of the high priority index, within the two peninsular plateaus and the middle South inland of Portugal. Such situation concurs with maximum to high deposition and maximum to high radiological vulnerability indexes. Compared to the high indexes distribution of the radiological vulnerability map, this high priority indexes show a smaller extension, specifically in those areas affected by medium deposition, located at the North-West area of central Spain, the North-East area below the Pyrenees, near the Mediterranean area and the South of Portugal.

It should be noted that the area of maximum radiological vulnerability (North-East in Figure 12) presents a medium prioritisation index in Portugal and a dominant low one in the Spanish Northwest, due, in this case to the dominant influence of a low deposition. In the areas that show minimum priority indexes concur minimum deposition and minimum vulnerability indexes.

**Figure 15.** From left to right: a) Deposition map, b) Radiological Vulnerability map and c) Prioritisation map. Projection: UTM WGS84 Zone 33.



Source: Own elaboration, CIEMAT, 2021.

Figure 15 allows to give an overview of the three types of maps obtained with the methodology developed. For a given radionuclide ( $^{137}\text{Cs}$ , in this case) the deposition map (Figure 15a) shows how the deposition pattern is determined by meteorological conditions such as the wind distribution, following a South West-North East axis, in agreement with the shape of the density maps. The Iberian Peninsula is affected by different degrees of deposition severity.

The behaviour of this same radionuclide in the soil-rainfed cereal system, determines the radiological vulnerability map (Figure 15b), which is affected by the clay content and the potassium status in soil, as well as the root uptake capacity of the crop. The resultant prioritisation map shows how areas affected by the same quantity deposition give different radiological impacts depending on the vulnerability of the soil-crop system, allowing to categorise the areas where recovery actions need to be taken in a prioritised way. This map shows that high deposit values do not directly imply a greater radiological risk, it is necessary to know the transfer potential of the activity concentration to the crop in order to be able to assess properly the risk.

## 5 Discussion and Conclusions

The elaboration of nuclear risk maps is one of the ways that help to understand the impact of radioactive releases and to decide and establish actions to minimize its effects. They are tools to better assess the risks from radiological or nuclear releases, as they help to identify and categorise the areas most affected and where the application of remediation techniques to mitigate the consequences could be feasible and effective.

The importance of having in advance this information, as part of an emergency preparedness program to face a nuclear or radiological accident, not only refers to the early phase of the emergency, when quick decisions must be taken to establish protective measures. It is also very useful in the longer term, once the situation has become an existing exposure situation, in the assessment of the radiological impact of the affected area, helping decision-makers to categorise and prioritise those zones where the implementation of recovery actions could be feasible and effective.

Risk maps, are the result of the combination of the deposition of the radionuclides released and the soil vulnerability to the contamination, understood as the potential to transfer the activity concentration along the food chain.

Under the ANURE agreement, a methodology to assess the nuclear risk in Europe has been developed and trained. The methodology is based on the combined use of accurate information on the deposition probability of a released radionuclide from a large number of real weather situations and on the soil-plant transfer potential of the contamination along the food chain.

Taking into account: i) the meteorological conditions determining the dispersion and deposition pattern of the radionuclides released after a nuclear accident, ii) the deposition magnitude and probability iii) the soil potential to transfer the activity concentration to the crop and hence to the food chain and iv) the land use, a methodology to elaborate risk radiological maps for the food chain pathway has been presented. The methodology is based on two different developments:

- The first, with the objective to create a deposition map, covers the dispersion simulations and the estimation of the ground deposition patterns and its degree of severity to radiation exposure.
- The second, focuses on the production of the radiological vulnerability map, defined as its potential to transfer the activity concentration deposited on the soil to the population.

The combination of both outcomes allows to identify the areas where the remediation or recovery actions should be applied in a prioritised way.

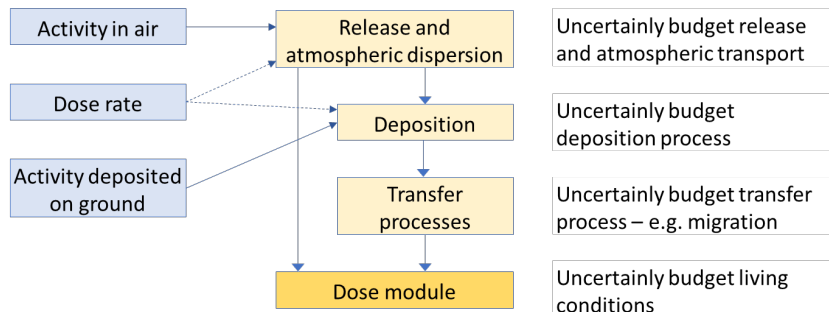
A case study for cereals and  $^{137}\text{Cs}$  deposition after an ISLOCA accident in Almaraz NPP has been taken as reference to train the methodology. This example highlights the importance of considering the local specificities since the dispersion pattern and deposition is highly influenced by geographic factors such as mountains and valleys, but not only. The type of soil and soil specific parameters that determine the soil potential to transfer the contamination to the crop and the food chain, are also decisive. The resultant prioritisation map shows how areas affected by the same quantity deposition arise in different risk, due to different soil-crop potential to transfer the contamination along the food chain: in other words, high deposit values do not directly imply a greater radiological risk; it is necessary to know the transfer potential of the activity concentration to the crop in order to be able to assess the risk properly. The map, that categorises the radiological risk, can be very useful as a guide in the decision-making process in order to plan and implement, in a prioritised way, the recovery actions to recover normal living conditions.

In selecting the modelling settings, the input data and their treatment, and the analysis of the results obtained in each assessing step, some sources of uncertainty have been encountered.

From the modelling point of view of the dispersion of radioactive material in the atmosphere and its deposition, it is worth noting that atmospheric dispersion models rely on the accuracy of the source term and the available meteorological information, i.e. how close this input information is to true values. Hence, it is easy to understand that the present study and results are subjected to uncertainties. In case of accidental dispersion of radionuclides into the atmosphere from a nuclear power plant, there are two main big sources of uncertainties: the weather forecast, and the source term. In other words, one uncertainty is associated with the meteorological data employed, and the other with the temporal evolution of the amount and physical/chemical properties of the release (Sørensen, 2020). In addition, and at the same level of importance, it is not possible to forget the intrinsic uncertainty of atmospheric and dispersion models due to assumptions made in physical model formulations and parameters (Rao, 2005), which can cause, for instance, to forecast different scenarios under the same set of meteorological and source term inputs. As an example of this

impact in the DSS used in the present study (JRODOS), Figure 16 gives an overview of the DSS model chain and related uncertainty budgets.

**Figure 16.** JRODOS model chain with connected uncertainty budgets and most relevant monitoring data to reduce uncertainties.



Source: Bleher et al., 2020

Small errors in the initial conditions and in the model calculations can result in incorrect forecasts at later times. Nevertheless, an estimation of a source term may lead to very different results, even for the same accident and the same plant because of the uncertainties associated to the release models, which are very complex, and not fully validated experimentally. Besides, the larger the period of time to be forecasted, the higher the uncertainties are. In the same line, due to the atmosphere being a non-linear system, even considering as input the best possible initial conditions and the most accurate numerical weather prediction model, uncertainties driving meteorology are inevitable, and hence, small initial errors can grow rapidly thus resulting in incorrect long-range forecasts.

Aiming to overcome the impact of relevant uncertainties, from the source term point of view, it is always recommended to carry out some sensitivity study on the most important parameters that may affect the source term, such as iodine chemistry, corium-concrete interaction, and even hydrogen generation. In the case of meteorological information the ensemble technique is widely used to model errors in the initial atmospheric state and in the model calculations, which is based on the simultaneous analysis of several model simulations by means of ad-hoc statistical treatments and parameters. Both would help to reduce the uncertainty in the decision-making process dealing with EP&R for nuclear and radiological emergencies.

Regarding the radiological vulnerability assessment, mean values for topsoil parameters are taken into account for the soil groups defined in (Trueba et al., 2015). Moreover, the resulting vulnerability maps would be dissimilar if a different attribution of soil properties or mapping units had been embraced. The use of the selected soil-to-plant transfer factors also introduces certain uncertainty since those values, empirically obtained, are simplified to their mean value. Therefore, a bunch of vulnerability maps may be performed considering all the possible combinations among the minimum and maximum transfer factor values and the minimum and maximum values for each soil group's topsoil parameters.

Another source of uncertainty in the soils' vulnerability assessment lies in the categories established to define the different indexes used along the methodological approach. This specifically relates to the number of categories defined for each index and the thresholds between categories used. This consideration also applies for the deposition map itself, since other deposition classes with different deposition weighting factors (which also affect these classes) would give different deposition maps. Moreover, it applies to the estimation of the prioritisation classes, as the combination between the *Radiological Vulnerability Index* and the *Deposition Index*.

The interpretation of the risk maps is also subject to uncertainties, depending on the end-users. The maps give a useful summary of the radiological situation and identify the areas where priority actions are needed. However, such as they have been displayed, they probably contain too much detailed information for certain stakeholders or decision makers that will request simplified information and undoubtedly are too complex to be used for communication to the public.

The ANURE project has proved to be a good platform to foster collaborations among groups. A very rich source of data has been created, and a set of flexible tools has been developed. The developed methodology combines improvements in the decision-making process to reduce uncertainties since it considers the local

specificities and helps to prioritise the areas where the remediation or recovery actions should be applied, being a useful tool in EP&R, as it can be applicable at any European spot.

This result is a valuable asset for nuclear EP&R, and it suggests the importance for having sufficient information prior to a radiological or nuclear event happens. The large amount of data produced under the ANURE project and already stored should support detailed studies.

## **6 Dissemination of project results**

The aim of this project is to promote cooperation in understanding and resolving nuclear EP&R issues from a multidisciplinary point of view, to develop procedures and promote methods to end-users, to exchange appropriate scientific knowledge in the nuclear EP&R and identify knowledge gaps in the analysis, quantification and communication of nuclear risk assessment.

Dissemination activities relating to the foreground of the project, scientific publication as well as the presentation of results in international forum/conferences have been accomplished during this period. The two research groups involved in the ANURE project have been actively collaborating with this purpose.

### **Scientific publications:**

#### **1. Seasonal variability assessment in the definition of priority action areas after a radioactive release.**

García-Puerta, B.; Sangiorgi, M.; Trueba Alonso, C.; Montero Prieto, M.; De Felice, L.; Hernández-Ceballos, M.A.  
In preparation.

#### **2. Chapter 19. Nuclear Accidents.**

Hernandez Ceballos, M.A.; Trueba Alonso, C.; Montero Prieto, M.C.; Iurlaro, G.; Sangiorgi, M.; García Puerta, B.  
In: Poljansek, K., *et al.*, 2021. Recommendations for National Risk Assessment for Disaster Risk Management in EU: Where Science and Policy Meet, Version 1, EUR 30596 EN, Publications Office of the European Union, Luxembourg, 2021, ISBN 978-92-76-30256-8, doi:10.2760/80545, JRC123585.  
<https://publications.jrc.ec.europa.eu/repository/handle/JRC123585>

#### **3. Dispersion and ground deposition of radioactive material according to airflow patterns for enhancing the preparedness to N/R emergencies.**

Hernández-Ceballos, M.A.; Sangiorgi, M.; García Puerta, B.; Montero, M.; Trueba, C.  
Journal of Environmental Radioactivity, 216, 106178, 2020. <https://doi.org/10.1016/j.jenvrad.2020.106178>.

#### **4. Seasonality influence in the elaboration of risk maps associated to the transfer of radioactivity through the food chain.**

Montero Prieto, M.; Trueba Alonso, C.; Sangiorgi, M.; García Puerta, B.; Hernández Ceballos, M.A.; De Felice, L.  
Proceedings of the 5<sup>th</sup> NERIS Workshop, 3-5 April 2019, Roskilde, Denmark.  
<https://www.eu-neris.net/all-documents/proceedings/262-neris-proceedings-2019.html>

#### **5. Chapter 15. Nuclear Accidents.**

Hernandez Ceballos, M.A.; Trueba Alonso, C.; Montero Prieto, M.C.; Iurlaro, G.; Sangiorgi, M.; García Puerta, B.  
In: Poljanšek, K. *et al.*, 2019. Recommendations for National Risk Assessment for Disaster Risk Management in EU: Approaches for identifying, analysing, and evaluating risks. Version 0. EUR 29557 EN, Publications Office of the European Union, Luxembourg, 2019, ISBN 978-92-79-98366-5 (online), doi:10.2760/084707 (online), JRC114650.  
<https://publications.jrc.ec.europa.eu/repository/handle/JRC114650>.

#### **6. ANURE project: Towards the implementation of a nuclear risk assessment methodology.**

García Puerta, B.; Sangiorgi, M.; Hernández-Ceballos, M.A.; Trueba Alonso, C.; De Felice, L.; Montero Prieto, M.

Proceedings of the 4<sup>th</sup> NERIS Workshop, 25-27 April 2018, Dublin, Ireland. (pp 73-80). ISBN 978-2-9552982-2-0. <https://www.eu-neris.net/library/proceedings/182-4th-neris-workshop-proceedings/file.html>

## **7. Wind field characterization to improve evaluation criteria for radiological monitoring networks.**

Hernández Ceballos, M.A.; De Felice, L.; De Cort, M.

Proceeding of the 3<sup>rd</sup> NERIS Workshop, 17-19 May 2017, Lisbon, Portugal. (pp 46-49). ISBN 978-2-9552982-1-3. [https://www.eu-neris.net/images/activities/workshops/2017-05/proceedings\\_NERIS\\_workshop\\_2017.pdf](https://www.eu-neris.net/images/activities/workshops/2017-05/proceedings_NERIS_workshop_2017.pdf)

### **Conferences:**

#### **1. Nuclear risk assessment methodology to support the planning and management of post-accident recovery. ANURE Project.**

García- Puerta, B.; Trueba Alonso, C.; Montero Prieto, M.; Hernández-Ceballos, M.A.; Sangiorgi, M.

ICRP International Conference on Recovery after Nuclear Accidents. Radiological Protection Lessons from Fukushima and Beyond. (Virtual), 1-4 December 2020. (Oral + paper).

<https://www.icrprecovery.org/post/cp-34>

#### **2. Dispersion and ground deposition characteristics of radioactive material according to air mass classification for enhancing the preparedness to N/R emergencies.**

Hernández-Ceballos, M.A.; Sangiorgi, M.; García Puerta, B.; Montero, M.; Trueba, C.

5<sup>th</sup> International Conference on Environmental Radioactivity ENVIRA 2019: Variations of Environmental Radionuclides, Praha, Czech Republic, 8-13 September 2019. In: Světlík, I.; Povinek, P.; Pachnerová, K., Eds. ENVIRA 2019 Proceedings. Czech Technical University in Prague, 2019. ISBN 978-80-01-06692-8. <https://doi.org/10.14311/ENVIRA.2019>. <http://hdl.handle.net/10467/86886>

#### **3. Desarrollo de mapas de riesgos como herramienta de ayuda en el establecimiento de estrategias de recuperación de zonas contaminadas radiológicamente [Development of risk maps as a tool to assist in the establishment of recovery strategies for radiologically contaminated areas] (In Spanish).**

García-Puerta, B.; Sangiorgi, M.; Hernández-Ceballos, M.A.; Trueba, C.; Montero, M.; De Felice, L.

6º Congreso conjunto SEFM/SEPR, Burgos, Spain, 11-14 June 2019. (Oral).

<https://plataforma.congresosefmsepr.es/event/1/contributions/205/>

#### **4. Seasonality influence in the elaboration of risk maps associated to the transfer of radioactivity through the food chain.**

Montero Prieto, M.; Trueba Alonso, C.; Sangiorgi, M.; García Puerta, B.; Hernández Ceballos, M.A.; De Felice, L.

5<sup>th</sup> NERIS Workshop, Roskilde, Denmark, 3-5 April 2019. (Oral).

<https://www.eu-neris.net/activities/workshops/42-presentations/202-5th-neris-workshop-presentations.html>

#### **5. Enhance the decision-making process to minimize the impact in agricultural areas derived from a nuclear accident.**

García Puerta, B.; Trueba Alonso, C.; Montero Prieto, M.

3<sup>rd</sup> European Radiological Protection Research Week (ERPW), Rovinj – Rovigno, Croatia, 1-5 October 2018. (Oral). In: Surić Mihić, M. and Prlić, I., Eds., 2018. Book of Abstracts. Institute for medical research and occupational health (IMI), Zagreb, Croatia. (p 168).

**6. Mapas de riesgo nuclear: una herramienta para la racionalización de los planes de recuperación posaccidente [Nuclear risk maps: a tool for rationalisation post-accident recovery plans] (In Spanish).**

García Puerta, B.; Sangiorgi, M.; Hernández-Ceballos, M.A.; Trueba Alonso, C.; Montero Prieto, M.; De Felice, L.

44<sup>a</sup> Reunión Anual de la Sociedad Nuclear Española, Ávila, Spain, 26-28 September 2018. (Oral).

**7. Assessing contamination probability following a severe accident in a Spanish Nuclear Power Plant.**

García Puerta, B.; Hernández-Ceballos, M.A.; Trueba Alonso, C.; De Felice, L.; Sangiorgi, M.; Montero Prieto, M.

RODOS User Group Meeting 2018, Munich, Germany, 14-15 May 2018. (Oral).

**8. ANURE project: Towards the implementation of a nuclear risk assessment methodology.**

García Puerta, B.; Hernández-Ceballos, M.A.; Trueba Alonso, C.; De Felice, L.; Sangiorgi, M.; Montero Prieto, M.

4<sup>th</sup> NERIS Workshop, Dublin, Ireland, 25-27 April 2018. (Oral).

<https://www.eu-neris.net/activities/workshops/dublin-2018.html>

**9. European nuclear Risk Mapping by Kernel Density Estimation applied to air mass trajectories.**

Hernández Ceballos, M.A.; De Felice, L.; De Cort., M.

NERIS Workshop 2017, Lisbon, Portugal, 17-19 May 2017. (Oral Presentation).

<https://www.eu-neris.net/activities/workshops/lisbon-2017.html>

**10. Local factors to make risk maps, for potential nuclear accident affected farming areas, to be applied in the decision-making process.**

García Puerta, B.; Trueba Alonso, C.; Montero Prieto, M.

4<sup>th</sup> International Conference on Radioecology and Environmental Radioactivity (ICRER), Berlin, Germany, 3-8 September 2017. (Poster). In: Institut de Radioprotection et de Sécurité Nucléaire, 2017. Abstracts Book (pp 185-186). ISBN 978-2-9545237-7-4.

## References

- Bleher, M., Gering, F., Stohlker, U., et al., 2020. Reduction of uncertainties in exposure assessment based on environmental monitoring data. Radioprotection 2020, 55(HS1), S81–S88.  
<https://doi.org/10.1051/radiopro/2020016>
- Baklanov A. (Ed.), 2003. Evaluation of doses, risks, vulnerabilities and consequences for population and environment in Euro-Arctic Region, DMI Sci.Report 03-18, 68p; pp. 40–55
- Christoudias, T., Proestos, Y., Lelieveld,J., 2014. Global risk from the atmospheric dispersion of radionuclides by nuclear power plant accidents in the coming decades. Atmos. Chem. Phys., 14, 4607–4616.
- CNAT, 2020. Environmental Report 2019. Centrales Nucleares Almaraz-Trillo, Ed..
- Domínguez Vivancos, A., 1997. Tratado de Fertilización. Ed Mundiprensa. ISBN 84-7114-622-3. Page 161.
- EC-ESBN, 2004. European Commission and the European Soil Bureau Network, CD-ROM, EUR 19945 EN. The European Soil Database distribution version 2.0. [Online] Available at: <https://esdac.jrc.ec.europa.eu/resource-type/european-soil-database-soil-properties>
- EEA, 2016. Corine Land Cover 2012 seamless vector data. 2016. Version 18\_5. [Online] Available at: [https://data.europa.eu/euodp/en/data/dataset/data\\_clc-2012-vector](https://data.europa.eu/euodp/en/data/dataset/data_clc-2012-vector)
- ESRI, 2016. ArcGIS Desktop: Release 10.5. Environmental Systems Research Institute, Redlands, CA.
- Fann, N., Brennan, T., Dolwick, P., Gamble, J.L., Ilacqua, V., Kolb, L. et al., 2016. Air Quality Impacts. In: Program GCR, editor. Impacts Clim. Chang. Hum. Heal. United States A Sci. Assess. Washington, DC: Global Change Research Program. p. 69–98.
- Garcia-Puerta, B., 2020. The use of Geographic Information Systems in creating tools to improve nuclear emergency and response plans and as an aid in the decision-making process for agricultural áreas. [Doctoral Thesis, Complutense University of Madrid, Spain]. E-prints Complutense repository.  
<https://hdl.handle.net/20.500.14352/11474>.
- Gómez, A.G., Ondiviela, B., Puente, A., Juanes, J.A., 2015. Environmental risk assessment of water quality in harbor areas: A new methodology applied to European ports. Journal of Environmental Management, 155, 77–88.
- Hernández-Ceballos, M.A., Sangiorgi, M., García Puerta, B., Montero, M., Trueba, C., 2020. Dispersion and ground deposition of radioactive material according to airflow patterns for enhancing the preparedness to N/R emergencies. Journal of Environmental Radioactivity, 216, 106178.  
<https://doi.org/10.1016/j.jenvrad.2020.106178>
- IAEA, 2005. Environmental and source monitoring for purposes of radiation protection Specific Safety Guidelines. IAEA, Safety standards series nº RS-G-1.8.
- IAEA, 2010. Handbook of parameter values for the prediction of radionuclide transfer in terrestrial and freshwater environments. IAEA, Technical reports series nº 472.
- IAEA, 2016. IAEA Safety Glossary. Terminology Used in Nuclear Safety and Radiation Protection (2016 Revision), 219 pp.
- Kalthoff, N., Bischoff-Gauss, L., Fiedler, F., 2003. Regional effects of large-scale extreme wind events over orographically structured terrain. Theoretical and Applied Climatology 74, 53 - 67.
- Karlsruhe Institute of Technology (KIT), 2017. JRodos Customer Guide. Version 3.0. February 2017. Pages 24.
- Lauritzen, B. (2007). Nuclear risk from atmospheric dispersion in Northern Europe - Final report of the NKS-B project NordRisk. 2005-2006. Roskilde. NKS (NKS-158).
- Lauritzen, B. (2011). Nuclear risk from atmospheric dispersion in Northern Europe - Summary Report. Roskilde: NKS. (NKS-244).
- Lelieveld, J., Kunkel, D., Lawrence, M.G., 2012. Global risk of radioactive fallout after major nuclear reactor accidents. Atmos. Chem. Phys., 12, 4245–4258.
- Levy, I., Dayan, U., Mahre, Y., 2010. Differing atmospheric scales of motion and their impact on air pollutants. International Journal of Climatology, 30, 612–619.

Nisbet A.F., Woodman R.F.M., 1998. Recommended soil-to-plant transfer factors for radiocaesium and radiostrontium for use in arable systems. National Radiological Protection Board. Chilton Didcot. Oxon OX11 ORQ, United Kingdom. TEMAS Technical Deliverable Version. 3. Project FI4P-CT95-0021 b (PL950220). 4<sup>th</sup> Framework Programme Nuclear Fission Safety of the European Commission.

Nisbet, A.F., Woodman, R.F.M., 2000. Soil-to-Plant transfer factors for radiocaesium and radiostrontium in agricultural systems. *Health Physics* 78, 279-288.

Nordic Guidelines and Recommendations (NGR), 2014. Protective Measures in Early and Intermediate Phases of a Nuclear or Radiological Emergency. Beredskabsstyrelsen (Denmark), Sundhedsstyrelsen (Denmark), Geislavarnir Rikisins (Iceland), Stuk (Finland), Statens Stralevern (Norway), Stral Sakerhets Myndigheten (Sweden).

NOAA National Centers for Environmental Prediction (NCEP). 2011. NOAA/NCEP Global Forecast System (GFS) Atmospheric Model. [2012-2016.] Distributed by the Pacific Islands Ocean Observing System (PaCOOS). [http://pacioos.org/metadata/ncep\\_global.html](http://pacioos.org/metadata/ncep_global.html). Accessed [2017].

Nuclear Regulatory Commission (U.S.) (NRC), 2013. State-of-the-Art Reactor. Consequence Analyses Project (SOARCA) NUREG-1935 (NUREG/CR-7110, Vol. 2, Rev. 1): Surry Integrated Analysis. Albuquerque, New Mexico 87185, USA. U.S. Department of Energy. Office of Nuclear Regulatory Research.

OECD/NEA, 2010. Strategic Aspects of Nuclear and Radiological Emergency Management. Planning for Effective Decision Making; Consequence Management and Transition to Recovery. Radiological Protection NEA № 6387. OECD Publications, France. 2010. ISBN 978-92-64-99146-0. Available online at: [https://www.oecd-nea.org/jcms/pl\\_14412](https://www.oecd-nea.org/jcms/pl_14412)

Pérez, I.A., Artuso, F., Mahmud, M., Kulshrestha, U., Sánchez, M.L., García, M.A., 2015. Applications of Air Mass Trajectories. *Advances in Meteorology* Volume 2015, Article ID 284213, 20 pages.

Poljansek, K., Casajus Valles, A., Marin Ferrer, M., Artes Vivancos, T., Boca, R., Bonadonna, C., Branco, A., Campanharo, W., De Jager, A., De Rigo, D., Dottori, F., Durrant, T., Estreguil, C., Ferrari, D., Frischknecht, C., Galbusera, L., Garcia Puerta, B., Giannopoulos, G., Girgin, S., Gowland, R., Grecchi, R., Hernandez Ceballos, M.A., Iurlaro, G., Kampourakis, G., Karlos, V., Krausmann, E., Larcher, M., Lequarre, A.S., Liberta', G., Loughlin, S.C., Maianti, P., Mangione, D., Marques, A., Menoni, S., Montero Prieto, M., Naumann, G., Necci, A., Jacome Felix Oom, D., Pfieffer, H., Robuchon, M., Salamon, P., Sangiorgi, M., San-Miguel-Ayanz, J., Raposo De M. Do N. E S. De Sotto Mayor, M.L., Theocharidou, M., Theodoridis, G., Trueba Alonso, C., Tsionis, G., Vogt, J. and Wood, M., 2021. Recommendations for National Risk Assessment for Disaster Risk Management in EU, EUR 30596 EN, Publications Office of the European Union, Luxembourg, ISBN 978-92-76-30256-8, doi:10.2760/80545, JRC123585. <https://publications.jrc.ec.europa.eu/repository/handle/JRC123585>

Rao, K.S. Uncertainty Analysis in Atmospheric Dispersion Modeling. *Pure appl. geophys.* 162, 1893–1917 (2005). <https://doi.org/10.1007/s00024-005-2697-4>

Seibert, P., Arnold, D., Arnold, N., Gufler, K., Kromp-Kolb, H., Mraz, G., Sholly, S., Wenisch, A., 2013. flexRISK – Flexible Tools for Assessment of Nuclear Risk in Europe Final Report (Version May 2013). Institut für Meteorologie (BOKU-Met), Department Wasser – Atmosphäre – Umwelt, Universität für Bodenkultur Wien. ISSN 1994-4187 (on-line).

Sevelyeva, E., Panchenko, S., 2012. Comparison of the Chernobyl and Fukushima Nuclear Power Plants Accidents and their Consequences. 6<sup>th</sup> International Congress on Environmental Modelling and Software, Modelling and Software, Leipzig, Germany, July 2012.

Shi, X., 2010. Selection of bandwidth type and adjustment side in kernel density estimation over inhomogeneous backgrounds. *Journal International Journal of Geographical Information Science*, 24:5, 643-660.

Sørensen, J. H., Barwicki, J., Blixt Buhr, A. M., Feddersen, H., Cordt Hoe, S., Israelson, C., Klein, H., Lauritzen, B., Lindgren, J., Schönfeldt, F., Sigg, R., Uncertainties in atmospheric dispersion modelling during nuclear accidents, *Journal of Environmental Radioactivity*, Volume 222, 2020.

Srinivas, C.V., Venkatesan, R., Baskaran, R., Rajagopal, V., Venkatraman, B., 2012. Regional scale atmospheric dispersion simulation of accidental releases of radionuclides from Fukushima Dai-ichi reactor. *Atmos Environ.*, 61, 66-84.

Stein, A.F., Draxler, R.R., Rolph, G.D., Stunder, B.J.B., Cohen, M.D., and Ngan, F., 2015. NOAA's HYSPLIT atmospheric transport and dispersion modeling system, *Bull. Amer. Meteor. Soc.*, 96, 2059-2077.

- Steinhauser, G., Brandl, A., Johnson, T.E., 2014. Comparison of the Chernobyl and Fukushima nuclear accidents: A review of the environmental impacts. *Science of the Total Environment*, 470–471, 800-817.
- Thykier-Nielsen, S., Deme, S., Mikkelsen, T., 1999. Description of the Atmospheric Dispersion Module RIMPUFF. RODOS(WG2)-TN(98)-02.
- Toledano, C., Cachorro, V.E., De Frutos, A.M., Torres, B., Berjón, A., Sorribas, M., Stone, R.S., 2009. Airmass classification and analysis of aerosol types at El Arenosillo (Spain). *Journal of Applied Meteorology and Climatology*, 48, 962-981.
- Trueba C., Vallés O., 2000. Evaluación de la Vulnerabilidad Radiológica de los Suelos Españoles para la Recuperación Ambiental tras Accidente Nuclear. Iniciativa ATYCA. CIEMAT/DIAE/51620/01-00.
- Trueba C., 2004. Metodología para evaluar la sensibilidad radiológica de suelos y su aplicación a los suelos peninsulares españoles. Tesis Doctoral. Departamento de Ingeniería Nuclear. Escuela Técnica Superior de Ingenieros Industriales. Universidad Politécnica de Madrid.
- Trueba, C., Garcia-Puerta, B., Montero M., 2015. Mapas de vulnerabilidad radiológica. Actualización al nuevo mapa europeo de suelos. ISBN:978-84-7834-749-0. Madrid, Spain: CIEMAT.
- Wu, X., Lu, Y., Zhou, S., Chen, L., Xu, B., 2016. Impact of climate change on human infectious diseases: empirical evidence and human adaptation. *Environ. Int.*, 86, pp. 14-23.

## **List of abbreviations and definitions**

ADM	Atmospheric Dispersion Model
AEMET	Agencia Estatal de Meteorología – Spanish Meteorological Agency.
CA	Collaboration Agreement
CIEMAT	Centro de Investigaciones Energéticas, Medioambientales y Tecnológicas
CSV	Comma Separated Files
DEM	Digital Elevation Model
DSS	Decision Support System
EC	European Commission
EEA	Environmental European Agency
EP	Emergency Preparedness
EP&R	Emergency Preparedness and Response
EU	European Union
GFS	Global Forecast System
GIS	Geographical Information System
JRC	Joint Research Centre
LTSBO	Long Term Station Black-Out
MITECO	Ministerio para la Transición Ecológica y el Reto Demográfico – Spanish Ministry for the Ecological Transition and the Demographic challenge.
MRF	Medium Range Forecast
NCEP	National Centres for Environmental Prediction
NEA	OECD Nuclear Energy Agency
NOAA	National Oceanic and Atmospheric Administration (of United States of America)
NOMADS	NOAA Operational Model Archive and Distribution System
NPP	Nuclear Power Plant
N/R	Relative to nuclear or radiological events
NWP	Numerical Weather Prediction
OCDE	Organisation for Economic Co-operation and Development
SA	Specific Agreement
SOARCA	State-of-the-Art Reactor Consequence Analyses
ST	Source Term
TF	Transfer factor soil to plant
US	United States (of America)
WMO	World Meteorological Organization

## List of figures

- Figure 17.** Methodological design of the risk assessment and mapping processes in ANURE. 11
- Figure 18.** Almaraz NPP site 15
- Figure 19.** Climograph of Almaraz site, Cáceres (Spain), 1972 to 2021. 16
- Figure 20.** Characteristic wind rose for the Almaraz NPP site including the distribution of the frequencies of wind speed and wind direction. 17
- Figure 21.** Density map for the period 2012-2016, as well as the corresponding seasonal density maps for the same period, i.e. Winter (from 22<sup>nd</sup> December to 21<sup>st</sup> March), Spring (from 22<sup>nd</sup> March to 21<sup>st</sup> June), Summer (from 22<sup>nd</sup> June to 21<sup>st</sup> September) and Autumn (from 22<sup>nd</sup> September to 21<sup>st</sup> December). 18
- Figure 22.** Estimation of the activity of  $^{131}\text{I}$ ,  $^{90}\text{Sr}$  and  $^{137}\text{Cs}$  released in time (hourly basis) for the ISLOCA (left-hand side) and LTSBO (right-hand side) sequence accidents. 19
- Figure 23.** Numerical grid for calculation used in the Almaraz case study. Projection: UTM WGS84 Zone 33. 20
- Figure 24.** Example of the  $^{131}\text{I}$  deposition [ $\text{Bq m}^{-2}$ ]. Projection: UTM WGS84 Zone 33 20
- Figure 25.** Probability analysis of the  $^{137}\text{Cs}$  deposited considering the simulations performed for an ISLOCA (left-hand side) and a LTSBO (right-hand side) accident scenarios in Almaraz NPP. The ranges of activity concentration deposited on ground are, from top to bottom, over  $0.01 \text{ kBq m}^{-2}$ , over  $0.1 \text{ kBq m}^{-2}$ , over  $1.0 \text{ kBq m}^{-2}$  and over  $10.0 \text{ kBq m}^{-2}$ . Projection: UTM ETRS89 Zone 30. 21
- Figure 26.** Annual  $^{137}\text{Cs}$  Deposition index average map (on the left) along 2012-2016 period (Projection: UTM WGS84 Zone 33); on the right, the map has been superimposed over an image of the Iberian Peninsula relief, showing the influence of the relief on the zoning 23
- Figure 27.** Matrix to define the *Radiological Vulnerability Index* and definitive values for this index: from 1 to 5 25
- Figure 28.** Radiological Vulnerability map. Projection: UTM WGS84 Zone 33 26
- Figure 29.** Matrix to define the Prioritisation of the agricultural contaminated areas facing their long-term recovery, by combining the *Deposition Index* and the *Radiological Vulnerability Index* 26
- Figure 30.** Prioritisation map for cereals and  $^{137}\text{Cs}$  deposition. Projection: UTM WGS84 Zone 33 . 27
- Figure 31.** From left to right: a) Deposition map, b) Radiological Vulnerability map and c) Prioritisation map. Projection: UTM WGS84 Zone 33 27
- Figure 32.** JRODOS model chain with connected uncertainty budgets and most relevant monitoring data to reduce uncertainties.. 30

## List of tables

<b>Table 1.</b> Main characteristics of the NCEP-GFS dataset.	13
<b>Table 2.</b> Contamination levels according to the activity concentration (kBq m <sup>-2</sup> ) of strong gamma and beta emitters deposited on ground	14
<b>Table 3.</b> Contamination levels considered in ANURE, with their corresponding activity concentration ranges of the total of strong gamma and beta emitters deposited on ground and the corresponding contribution of <sup>137</sup> Cs, and the Deposition Weighting Factors associated	19
<b>Table 4.</b> Caesium Bioavailability Index ( <i>I</i> _Cs) definition, considering clay and K soil content.	24
<b>Table 5.</b> Transfer factor values for grain cereals in temperate environments and the respective Soil-to-Crop Transfer Index assigned as function of the soil texture.	24

## Annexes

### Annex 1. Density maps calculation

The present methodology, which is based on the influence that lower atmosphere meteorology has on the dispersion and transport of substances in the atmosphere, is based on the calculation of density maps from the set of air mass trajectories for a period of 5 years (2012-2016) by applying the kernel density estimation method (Shi, 2010).

#### Trajectory modelling

Forward daily kinematic three-dimensional trajectories with duration of 120 hours and at different heights according with the case study (see section 3.1) were calculated for the 10-year period (2012-2016) by using the HYSPLIT model (Stein et al., 2015). The model computed air-mass locations (latitude, longitude and height above ground level) at 1-h intervals, i.e. trajectory endpoints.

To compute the trajectories, the 3-hourly meteorological archive data from NCEP's GDAS (National Weather Service's National Centers for Environmental Prediction - Global Data Assimilation System) were used. The GDAS covers from 2004 to the present, which is a big advantage in favour of using them in research studies, as they span 10 years or more. The GDAS is run 4 times a day, i.e., at 00, 06, 12, and 18 UTC. These data are archive and make available by the NOAA's Air Resources Laboratory (ARL) as 3 hourly, global, 1 degree latitude longitude dataset on pressure surface<sup>19</sup>.

#### Elaboration of Density maps from trajectories

Once calculated the trajectories and selected and stored the corresponding trajectory end-points for the period 2012-2016, the trajectory end-points within the entire period considered are extracted and displayed as density map using a kernel density estimating algorithm (Silverman, 1986).

Kernel density estimation (KDE) is an important method for mapping spatial patterns of point events and has application in many fields (ecology, public health, ). KDE is a non-parametric approach to the estimation of probability density functions using a finite number of samples (Krisp et al., 2009; Bartolini et al., 2013). To this purpose, this method fits a curved surface over each case (e.g. trajectory endpoint) such that the surface is highest above the centre and zero at a specified distance (the bandwidth) from the case. More information about differences between site-side and case-side calculations can be found in Shi 2010. Technically, the case-side method calculates the influence of the point of its vicinity, i.e. the distance around a case at which the influence of the endpoint is felt. This influence, over a two-dimensional space, can be represented as the following definition,

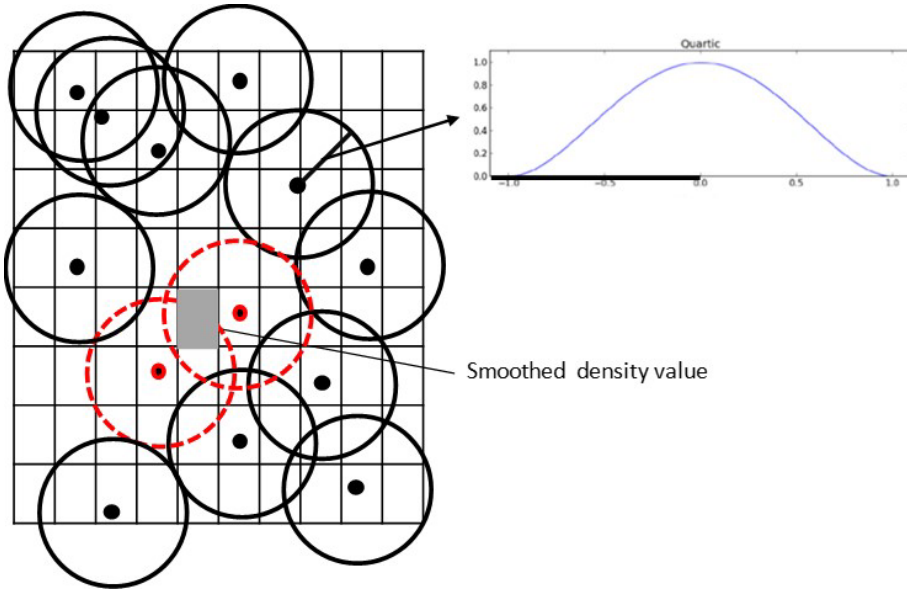
$$f(x, y) = \frac{1}{nh^2} \sum_{i=1}^n k\left(\frac{d_i}{h}\right)$$

where the  $f(x,y)$  is the density value at location  $(x,y)$ ,  $n$  is the total number of events points under concern,  $h$  is the bandwidth,  $d_i$  is the geographical distance between trajectory end-point  $i$  and location  $(x, y)$  and  $K$  is a density function (generally a radially symmetric unimodal probability density function) which integrates to one (Silverman, 1986; Shi, 2010).

Different kernel functions ( $k$ ) can be used, e.g. Cauchy kernel (Martin et al., 2004), Epanechnikov kernel (Lutz and Gutmann, 1995), Gaussian kernel (Connor and Hill, 1995). In the present study, the kernel function is based on the quartic kernel function described in Silverman (1986), i.e. an inverse distance weighting (Figure A1-1). More information about different kernel-smoothing algorithms can be found in Wand and Jones, 1995. In the present work, in addition, trajectories endpoints are displayed on a map with a fix grid cell size of 3 x 3 km and we have defined a bandwidth of 9 km.

<sup>19</sup> <https://www.ready.noaa.gov/gdas1.php>

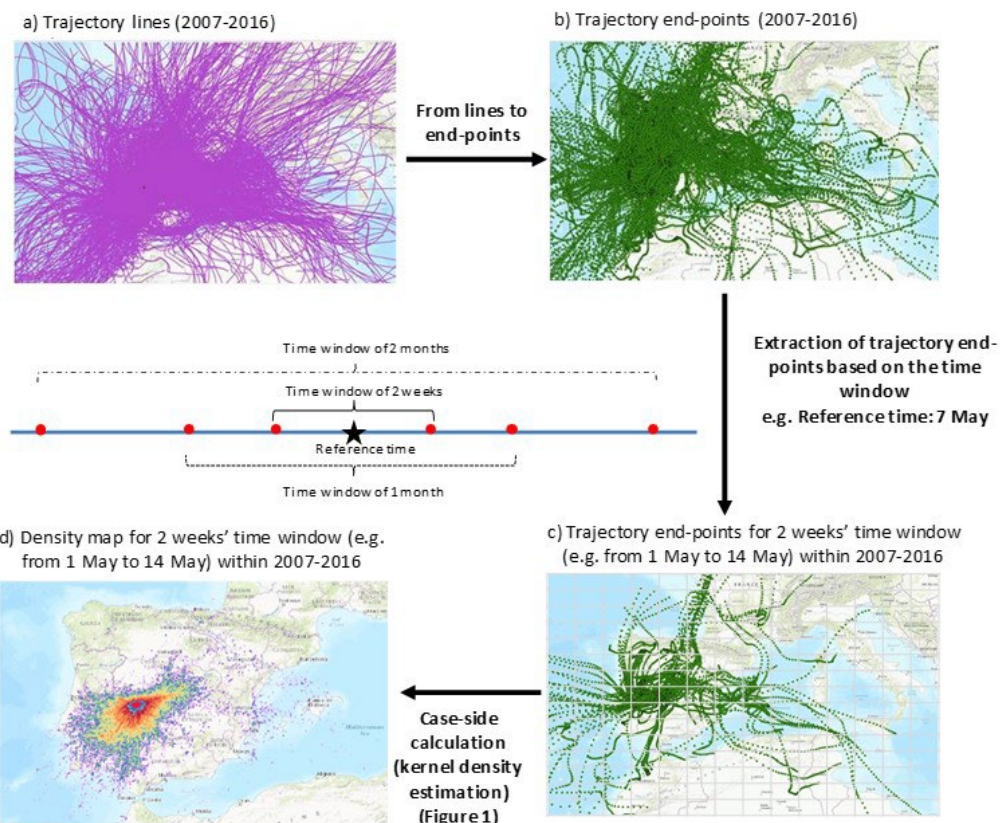
**Figure A1-1.** An illustration of the site-side calculations over raster data and the quartic kernel function used.



We define the “time window” as the reference period for which trajectory endpoints are collected and to which, as a result, the density map refers. This is used to calculate the set of seasonal density maps. We have taken winter (from 22<sup>nd</sup> December to 21<sup>st</sup> March), Spring (from 22<sup>nd</sup> March to 21<sup>st</sup> June), summer (from 22<sup>nd</sup> June to 21<sup>st</sup> September) and autumn (from 22<sup>nd</sup> September to 21<sup>st</sup> December).

Hence, those trajectory endpoints in the whole period 2012-2016 or within the selected time window are extracted to calculate the density map. Figure A1-2 shows the general procedure to determine the density at each output raster, which is based on the following steps: 1) calculate the set of trajectories for the 2007-2016 period at a certain location; 2) to split the trajectory lines (Figure A1-2a) into trajectory end-points (Figure A1-2b); 3) to define a regular grid covering the investigated region, with a fix grid cell size; 4) to define a bandwidth around the trajectory end-points (Figure A1-2c), 5) to obtain the smoothly curved surface over each trajectory end-point by applying the  $f(x,y)$  with the quartic kernel function (Figure A1-1); 6) to add the values of all the kernel surfaces where they overlap the raster cell centre (red circles and grey squared in Figure A1- 1) and 7) to plot the density layer in a density map (Fig A1-2d).

**Figure A1-2.** Steps and information used to produce the density maps: a) Set of trajectories lines and b) end-points for the 2007-2016 period, c) definition of time windows, and extraction of trajectory end-points for the defined time window (2 weeks), and d) example of density map.



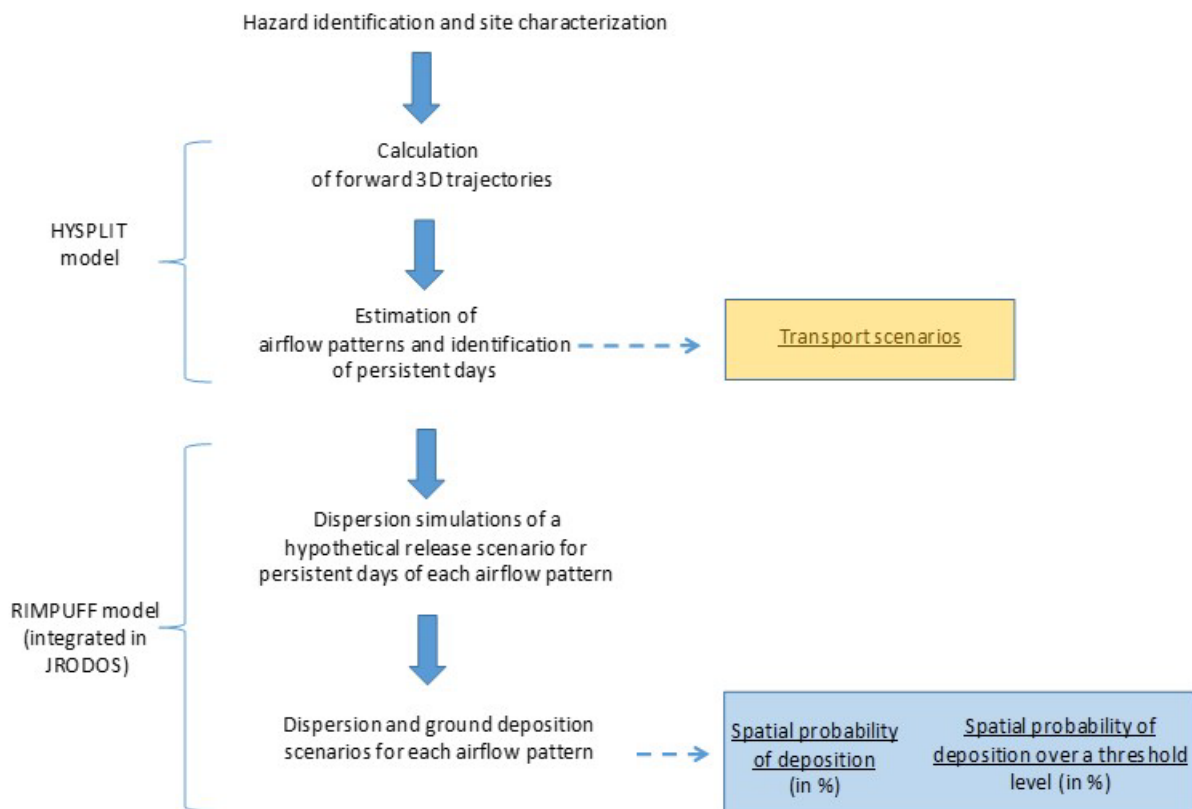
## References

- Bartolini, S., Cappello, A., Martí, J., Del Negro, C., 2013. QVAST: a new Quantum GIS plugin for estimating volcanic susceptibility. *Nat. Hazards Earth Syst. Sci.*, 13, 3031-3042.
- Connor, C. B. and Hill, B. E., 1995. Three non-homogenous Poisson models for the probability of basaltic volcanism: application to the Yucca Mountain region, Nevada, *J. Geophys. Res.*, 100, 10107-10125.
- Krisp, J.M., Peters, S., Murphy, C.E., Fan, H., 2009. Visual Bandwidth Selection for Kernel Density Maps. *Photogrammetrie Fernerkundung Geoinformation*, 5, 441-450.
- Lutz, T. M. and Gutmann, J. T.: An improved method for determining and characterizing alignments of point-like features and its implications for the Pinacate volcanic field, Sonoran, Mexico, *J. Geophys. Res.*, 100, 17659-17670, 1995
- Martin, A.J., Umeda, K., Connor, C.B., Weller, J.N., Zhao, D., Takahashi, M., 2004. Modeling long-term volcanic hazards through Bayesian inference: An example from the Tohoku volcanic arc Japan. *J.Geophys. Res.* 109.
- Shi, X., 2010. Selection of bandwidth type and adjustment side in kernel density estimation over inhomogeneous backgrounds. *Journal International Journal of Geographical Information Science*, 24:5, 643-660.
- Silverman, B.W., 1986. *Density Estimation for Statistics and Data Analysis*. New York: Chapman and Hall
- Stein, A.F., Draxler, R.R., Rolph, G.D., Stunder, B.J.B., Cohen, M.D., and Ngan, F., 2015. NOAA's HYSPLIT atmospheric transport and dispersion modeling system, *Bull. Amer. Meteor. Soc.*, 96, 2059-2077, <http://dx.doi.org/10.1175/BAMS-D-14-00110.1>
- Wand, M.P., Jones, M.C., 1995. *Kernel Smoothing Monographs on Statistics and Applied Probability* Chapman & Hall.

## Annex 2. Methodology to identify and characterize the dispersion and ground deposition of radioactive material according to airflow patterns

The methodology is trained based on the HYSPLIT trajectories (3644 forward trajectories) and RIMPUFF simulations (833 simulations) during five consecutive years (2012-2016) at the Almaraz Nuclear Power Plant. The methodology (Hernández-Ceballos et al., 2020) is shown in Figure A2-1.

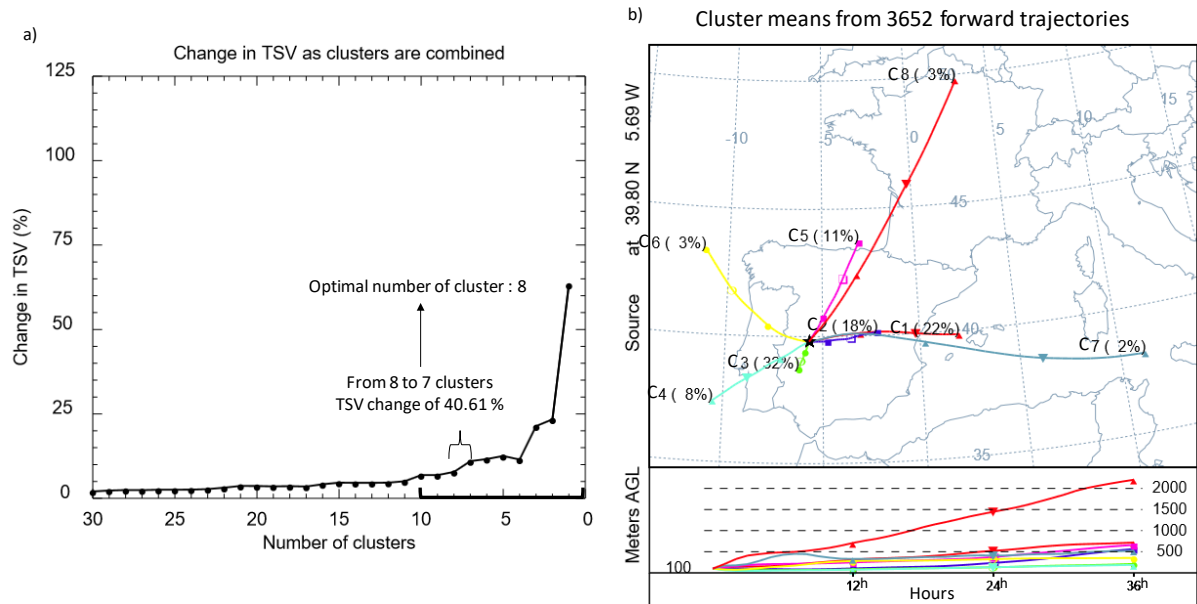
**Figure A2-1.** Flow diagram of the methodology combining air mass analysis and atmospheric dispersion simulations.



The database of air mass trajectories is composed by two kinematic 3D forward trajectories per day (00 and 12 UTC) with a run time of 36h at an initial height of 100 m above ground level (a.g.l.). Trajectories were grouped together in length and curvature by using the cluster methodology implemented in the HYSPLIT model. This method is based on variations of the total spatial variance (TSV) between the different clusters formed and the cluster spatial variance (CSV), with the purpose to minimize the differences among individual elements belonging to the same cluster and maximizes the differences among different clusters. The TSV is the sum of the CSV over all clusters. The process starts with N trajectories, and the clustering process continuously combines the two clusters that results in the minimum increase in TSV, until all trajectories are merged into one cluster. For each combination, the TSV is computed, and its variability along this process helps to identify the optimal number of clusters, which is defined as the number of clusters that best represents the air mass variability during one period. In the present methodology, this optimal number is associated with the first variation in percentage of the TSV above 40 % between two clusters in the range of the last ten combinations.

3644 forward trajectories (two per day at 00 and 12 UTC) were calculated from 2012 to 2016 at the ALM NPP. Figure A2-2a shows the variation (in percentages) of the TSV during the final 30 clustering merge combinations. The resulting optimal number of clusters is eight. Figure A2-2b provides the mean vertical and horizontal displacement of the eight cluster formed, and the percentage of trajectories included in each cluster (frequency of occurrence). In Figure A2-2b, there are five pronounced airflow patterns: to the east (C1, C2 and C7), to the north (C5 and C8), to the northwest (C6), to the southwest (C4) and nearby (C3).

**Figure A2-2.** a) Variation of the total spatial variance (TSV) with the number of clusters in the final 30 clustering merge combinations. b) Mean cluster pathways (centroids). The numbers on the right in the centroids are the percent of complete trajectories occurring in that cluster and the numbers on the left represent an identification number of the centroid.



From the total number of trajectories grouped in each cluster, the total number of persistent days, i.e. days in which trajectories at 00 and 12 UTC were grouped within the same cluster, is 1095 out of 1822 days (60%). Table A2-1 informs about the distribution of these days by airflow patterns, and its yearly distribution during 2012-2016.

**Table A2-1.** Number of trajectories and persistent days in each cluster, and yearly distribution of the persistent days during the 2012-2016 period.

	Eastern (E)			Northern (N)		Northwest (NW)	Southwest (SW)	Nearby (Nb)
Cluster	C1	C2	C7	C5	C8	C6	C4	C3
Number of pure days (%)	254	165	11	102	27	40	84	412
	(63 %)	(49 %)	(31 %)	(51 %)	(47 %)	(64 %)	(57 %)	(70 %)
Yearly distribution (counts)								
2012	51	46	0	19	2	5	13	85
2013	46	36	3	22	2	6	11	101
2014	61	38	1	26	5	4	12	86
2015	44	27	3	17	10	11	23	74
2016	52	18	4	18	8	14	25	66

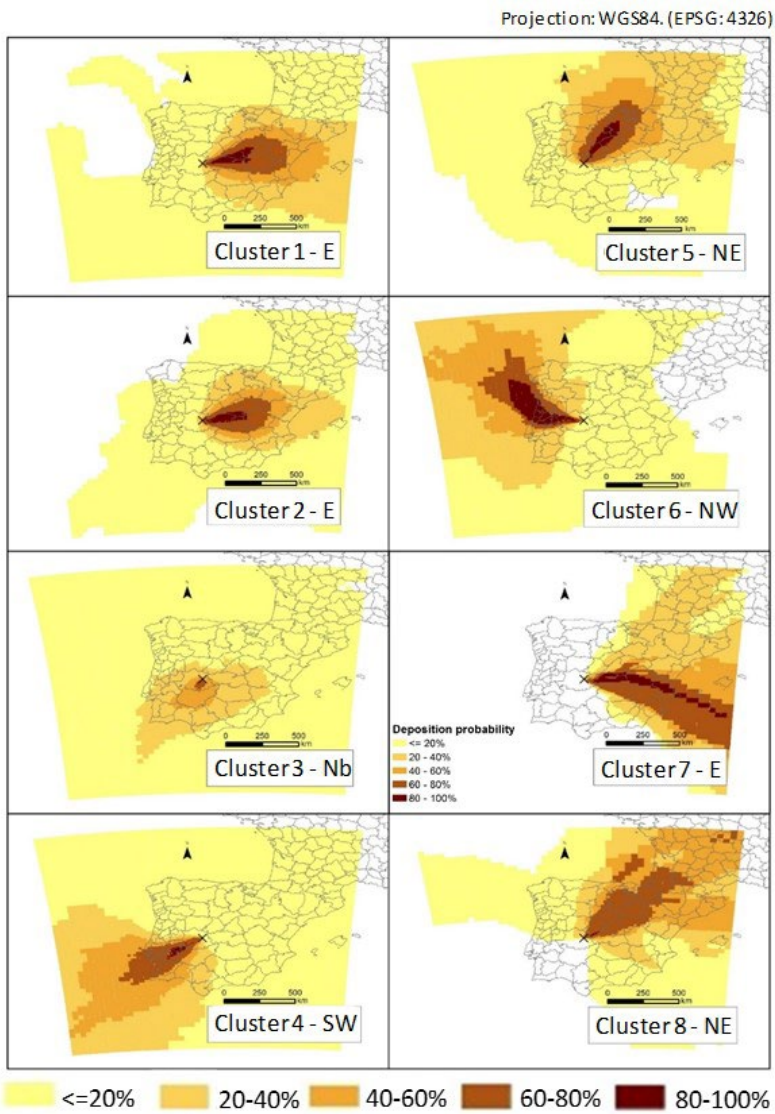
The statistical tool implemented in JRODOS was used to automatically performed the simulations during the 2012-2016 period. An interfacing systems loss-of-coolant accident (ISLOCA), initiated by an internal event caused by an unisolated rupture of low head safety injection piping outside containment, with 35 h of offsite radionuclide release was selected as accident sequence in this case study. The corresponding source term (considering  $^{131}\text{I}$ ,  $^{90}\text{Sr}$  and  $^{137}\text{Cs}$ ) has been obtained from the given release fractions for the classes of halogens, alkaline earths and alkali metals (USNRC, 2012), and grouped on an hourly basis, to which the inventory of  $^{131}\text{I}$ ,  $^{90}\text{Sr}$  and  $^{137}\text{Cs}$  of the ALM NPP, included in the JRODOS Database, was applied. Figure 4 shows the release fractions of these radionuclides during the ISLOCA accident. The stack height is 50 m and it was assumed a small heat flux so the effective release height was greater than 50 m.

Model outputs in each cell consisted of total ground deposition of specific radionuclides, such as  $^{131}\text{I}$ ,  $^{90}\text{Sr}$  and  $^{137}\text{Cs}$  ( $\text{Bq m}^{-2}$ ) at the end of each simulation.

Two analysis with respect to space are performed in order to estimate the affected areas by the radioactive deposition (location and the spatial coverage, in size and shape) over the whole simulation domain, in terms of occurrence and intensity:

- Probability of deposition: The probability of occurrence of depositions at every grid cell (Figure A2-3).

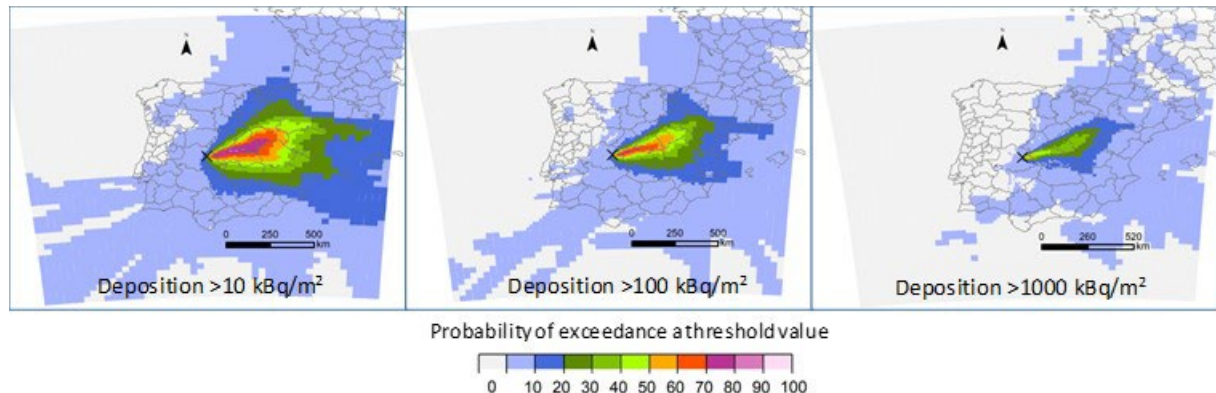
**Figure A2-3.** Spatial distribution of depositions for four clusters identified in Figure 2. The reference deposition values are taken at the end of each simulation. (83 hours)



- Probability of deposition over a threshold level: The probability of occurrence of depositions above a fixed activity concentration value, e.g. threshold of protective measures, at every grid cell (Figure A2-4).

Although these analyses are very simple, they allow condensing in a single representation the large amount of data, and hence, to outline the areas potentially more affected by depositions and the intensity and occurrence of these depositions. The method simplifies the complexity on the identification of the contamination pattern, and of those areas potentially affected and the activity concentration deposited. If an event were to happen, for instance, these results can be used to identify the corresponding airflow pattern, by accounting for the actual meteorological conditions during the accident, and then by scaling our unit emissions by the real release of radioactivity.

**Figure A2-4.** Spatial probability distribution of the eastern airflow (C1) pattern of being affected by total depositions over a) 10 kBq m<sup>-2</sup>, b) 100 kBq m<sup>-2</sup>, and c) 1000 kBq m<sup>-2</sup>. The reference deposition values are taken at the end of each simulation (83 hours).



The present method, with results from meteorological scenarios over five years in the analysis of air mass trajectories and in the characterization of dispersion and ground deposition, fits the need of guaranteeing the largest statistical sample and hence, the representativeness of the results to support decision-making. In addition, it leaves also room to increase the number of years in the future, as the meteorological files used in both span more than 10 years of high-resolution meteorological data. The possibility to progressively increase the number of trajectories/simulations enhances the statistical significance of the estimations obtained, and hence, enriches the decision-making process.

In general, this method provides comprehensive and oriented information and resources to decision makers to emergency management in terms of the most probable wind directions, and the possible affected areas by deposition, identifying the most vulnerable areas in terms of occurrence and intensity. If an event were to happen, for instance, these results can be used to identify the corresponding airflow pattern, by accounting for the actual meteorological conditions during the accident, and to estimate in advance the corresponding ground deposition pattern and intensity and then by scaling the estimated emissions by the real release of radioactivity.

#### Reference

Hernández-Ceballos, M.A., Sangiorgi, M., García Puerta, B., Montero, M., Trueba, C. Dispersion and ground deposition of radioactive material according to airflow patterns for enhancing the preparedness to N/R emergencies. *Journal of Environmental Radioactivity*, 216, 106178, 2020

**Annex 3. ISLOCA AND LTSBO source terms adapted to Almaraz NPP**

**Table A3-1.** ISLOCA Source Term (Bq)

Time (h)	$^{131}\text{I}$	$^{90}\text{Sr}$	$^{137}\text{Cs}$
13	1.35E+15	1.49E+11	2.52E+13
14	3.10E+17	1.57E+13	5.32E+15
15	4.30E+16	3.32E+12	5.60E+14
16	5.64E+15	1.16E+12	6.57E+13
17	1.72E+15	3.44E+11	2.21E+13
18	2.56E+13	5.13E+09	3.24E+11
20	1.48E+13	1.51E+10	1.65E+11
21	3.06E+13	1.95E+10	2.96E+11
22	4.13E+13	1.76E+10	3.87E+11
23	7.51E+13	1.45E+10	6.90E+11
24	1.91E+14	9.31E+09	1.73E+12
25	2.49E+14	3.15E+09	2.27E+12
26	8.77E+14	5.38E+09	7.97E+12
27	1.44E+15	1.28E+10	1.31E+13
28	7.11E+14	1.64E+09	6.45E+12
29	1.17E+15	3.92E+09	1.06E+13
30	9.90E+14	7.07E+09	8.96E+12
31	6.25E+14	1.48E+10	5.65E+12
32	1.37E+14	2.32E+10	1.26E+12
33	4.29E+13	5.20E+10	4.10E+11
34	3.91E+13	7.47E+10	4.01E+11
35	3.53E+13	1.24E+12	3.92E+11
36	6.10E+13	3.64E+12	6.81E+11
37	4.04E+13	3.49E+11	3.92E+11
38	7.83E+13	3.42E+11	7.57E+11
39	1.13E+15	4.50E+11	1.04E+13
40	4.84E+14	8.24E+10	4.43E+12
41	1.32E+14	1.69E+11	1.29E+12
42	2.38E+14	1.84E+11	2.29E+12
43	4.36E+14	1.98E+11	4.11E+12
44	4.06E+14	2.20E+11	3.85E+12
45	4.01E+14	2.77E+11	3.88E+12
46	2.05E+14	6.77E+10	1.97E+12
47	1.01E+14	6.10E+10	1.04E+12
<b>Total release</b>	<b>3.72E+17</b>	<b>2.83E+13</b>	<b>6.09E+15</b>

**Table A3-2.** LTSBO Source Term (Bq)

Time (h)	$^{131}\text{I}$	$^{90}\text{Sr}$	$^{137}\text{Cs}$
18	2.42E+13	2.25E+10	3.10E+12
22	4.84E+13	4.05E+11	6.20E+12
24	3.34E+13	1.28E+11	2.01E+12
45	8.76E+13	1.19E+11	1.08E+12
46	1.80E+14	2.32E+11	2.19E+12
47	3.00E+14	3.69E+11	3.63E+12
48	4.02E+14	4.88E+11	4.80E+12
49	4.69E+14	5.65E+11	5.55E+12
50	4.62E+14	5.56E+11	5.46E+12
51	4.74E+14	5.67E+11	5.55E+12
52	4.55E+14	5.42E+11	5.30E+12
53	4.31E+14	5.11E+11	4.96E+12
54	4.04E+14	4.77E+11	4.62E+12
55	3.80E+14	4.46E+11	4.31E+12
56	3.58E+14	4.19E+11	4.00E+12
57	3.39E+14	3.94E+11	3.75E+12
58	3.15E+14	3.65E+11	3.47E+12
59	2.95E+14	3.42E+11	3.22E+12
60	2.78E+14	3.20E+11	3.00E+12
61	2.64E+14	3.04E+11	2.82E+12
62	2.52E+14	2.86E+11	2.66E+12
63	2.39E+14	2.72E+11	2.50E+12
64	2.27E+14	2.59E+11	2.36E+12
65	2.16E+14	2.45E+11	2.22E+12
66	2.07E+14	2.34E+11	2.11E+12
67	2.02E+14	2.24E+11	2.04E+12
68	1.93E+14	2.05E+11	1.93E+12
69	1.85E+14	1.88E+11	1.83E+12
70	1.83E+14	1.79E+11	1.80E+12
71	1.14E+14	1.08E+11	1.12E+12
72	5.64E+12	5.22E+09	5.52E+10
<b>Total release</b>	<b>8.02E+15</b>	<b>9.77E+12</b>	<b>9.97E+13</b>

#### **Annex 4. Meteorological data**

Meteorological data were collected from the NOMADS (NOAA Operational Model Archive and Distribution System) free service provided by NOAA, the National Oceanic and Atmospheric Administration of United States of America. NOMADS is an FPT service where users can download anonymously Numerical Weather Prediction (NWP) files, an international standard which uses mathematical models of the atmosphere and oceans to predict the weather based on current weather conditions. The NWP files format used in this study is the GRIB2, an evolution of the GRIB format which is a WMO (World Meteorological Organization) standard for encoding gridded fields.

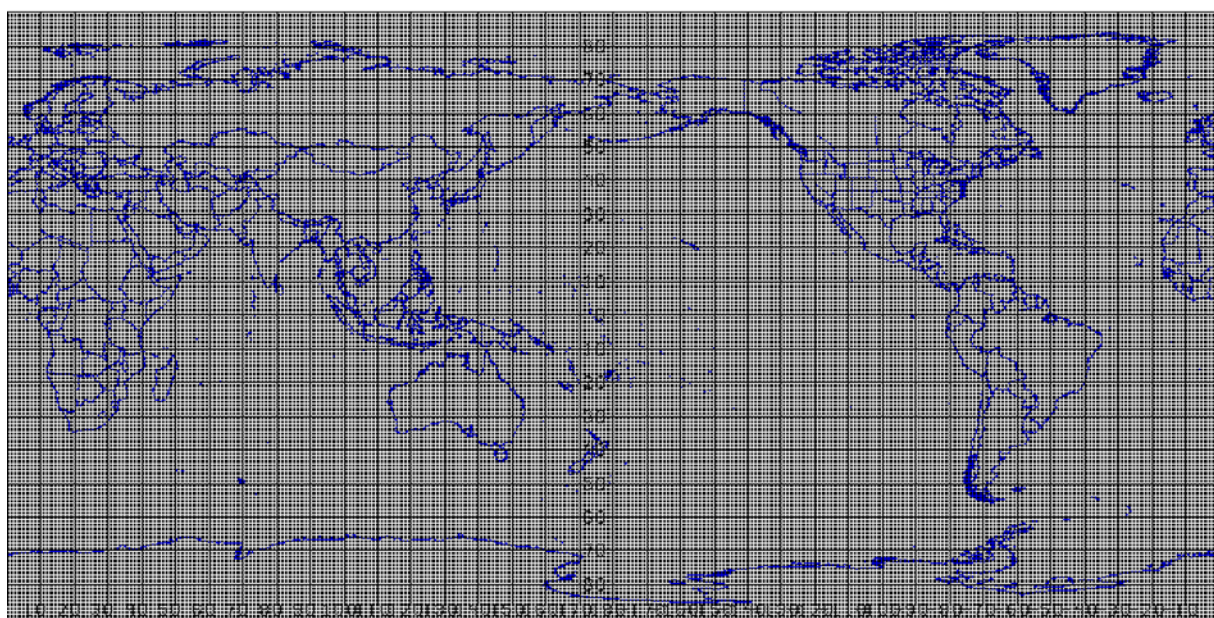
Several categories of model data are available through NOAA's National Operational Model Archive and Distribution System (NOMADS). These broad categories of data are Reanalysis, Numerical Weather Prediction, Climate Prediction, and Derived/Other Model Data. Model data are typically gridded data with varying temporal and spatial coverage. Model datasets can be thought of as three-dimensional cubes of weather information over a span of time. The kinds of weather information, resolution, coverage, and the period of record vary with each available dataset.

The Global Forecast System (GFS) is a weather forecast model produced by the National Centers for Environmental Prediction (NCEP). Dozens of atmospheric and land-soil variables are available through this dataset, from temperatures, winds, and precipitation to soil moisture and atmospheric ozone concentration. The entire globe is covered by the GFS at a base horizontal resolution of 18 miles (28 kilometres) between grid points (Figure A4-1), which is used by the operational forecasters who predict weather out to 16 days in the future. Horizontal resolution drops to 44 miles (70 kilometres) between grid point for forecasts between one week and two weeks.

The GFS model is a coupled model, composed of four separate models (an atmosphere model, an ocean model, a land/soil model, and a sea ice model), which work together to provide an accurate picture of weather conditions. Changes are regularly made to the GFS model to improve its performance and forecast accuracy. It is a constantly evolving and improving weather model. Gridded data are available for download through the NOAA National Operational Model Archive and Distribution System (NOMADS). Forecast products and more information on GFS are available at the GFS home page.

Prior to January 2003, the GFS was known as the GFS Aviation (AVN) model and the GFS Medium Range Forecast (MRF) model. GFS-AVN and MRF products are a collection from NCEP's NOAAport. Grids, domains, run frequencies, and output frequencies have changed over the years.

**Figure A4-1.** Domain of the GFS Analysis (GFS-ANL). Model grid 004 (0,5deg)



Source: NCEP NOAA-NCEP, 2007

## Annex 5. RIMPUFF ADM and EmergencyLite simulation

The dispersion calculations have been carried out with the Lagrangian mesoscale atmospheric dispersion puff model RIMPUFF, which is integrated in JRODOS Decision Support System. JRODOS has a library of models to cover most phases of the accident, from transport of radioactive material to deposition, countermeasures, doses, etc. Other ADMs available in JRODOS are DIPCOT<sup>20</sup> and LASAT<sup>21</sup>, both Lagrangian.

RIMPUFF, developed by Risø DTU National Laboratory for Sustainable Energy, Denmark, is equipped with computer-time effective features for stability dependant dispersion parameterization, plume rise formulas, inversion and ground-level reflection capabilities and wet/dry (source) depletion. It can be applied over moderate complex terrain by using a puff-splitting scheme in connection with external (to RIMPUFF) generated wind fields from separate wind modules.

The JRodos user interface to run the RIMPUFF model is illustrated by means of an example application. We have taken as reference the information included in KIT 2017.

Once the user Interface is open, we just click on the "Create a new project" icon; the EmergencyLite chain project shall be named Almaraz (Figure A5-1).

**Figure A5-1.** An image of GFS simulated total atmospheric ozone concentration



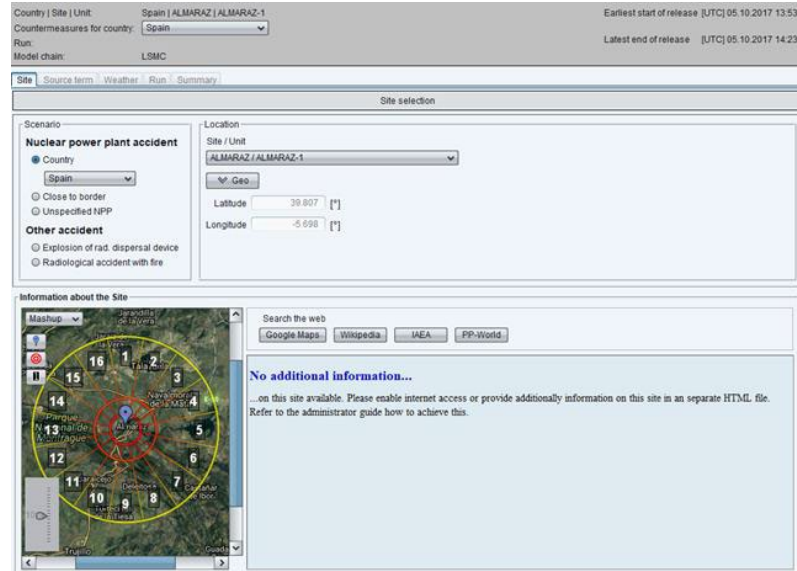
After clicking [OK], the RODOS-Lite Input Interface opens as a separate tab in the central window, and the operator must fill out a sequence of tabs before the calculation can be set on the way.

First step in JRODOS is to define the location of the desired NPP one wishes to study (Figure A5-2); from the list of available reactors in Spain, “Almaraz”, is the reactor for which the calculation shall be carried out. All operating NPP are already available in JRODOS database.

<sup>(20)</sup> [milos.ippt.demokritos.gr/DIPCOT.htm](http://milos.ippt.demokritos.gr/DIPCOT.htm)

<sup>(21)</sup> [www.janicke.de/en/lasat.html](http://www.janicke.de/en/lasat.html)

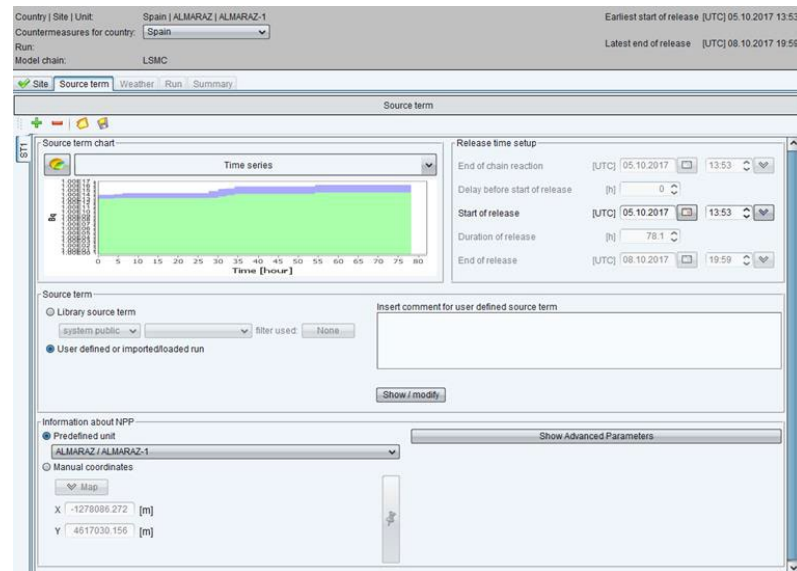
**Figure A5-2.** Site selection in JRODOS.



Once selected, it needs to click [OK] and it will be open the next tab, "Source term", in which the source term is defined (see Figure A5-3). We could use either the JRODOS "System public" source term library or to define the source term by ourselves. Under ANURE, we have specified by hand the source term explained in section 4.3.

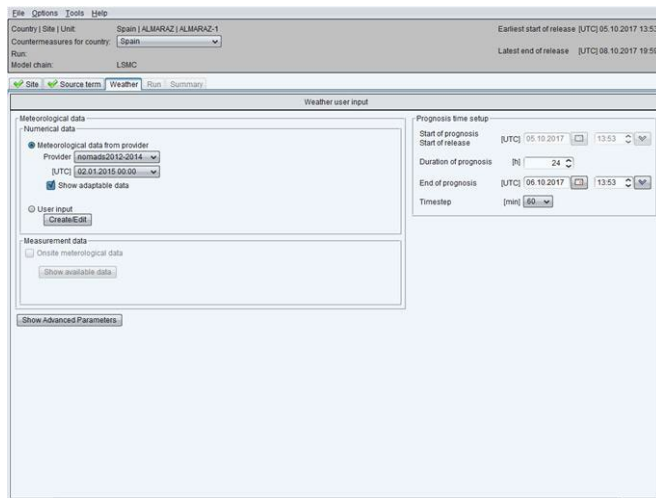
A descriptive text and a figure appear in the comment box and the "Source term chart" section. We can fix the date and time and selects source term, although, under ANURE, the start of release is not important as it is changed randomly by the statistic tool during calculation. In the "Weather" tab, the operator makes this specification in the "Prognosis time setup" section.

**Figure A5-3.** Source term selection.



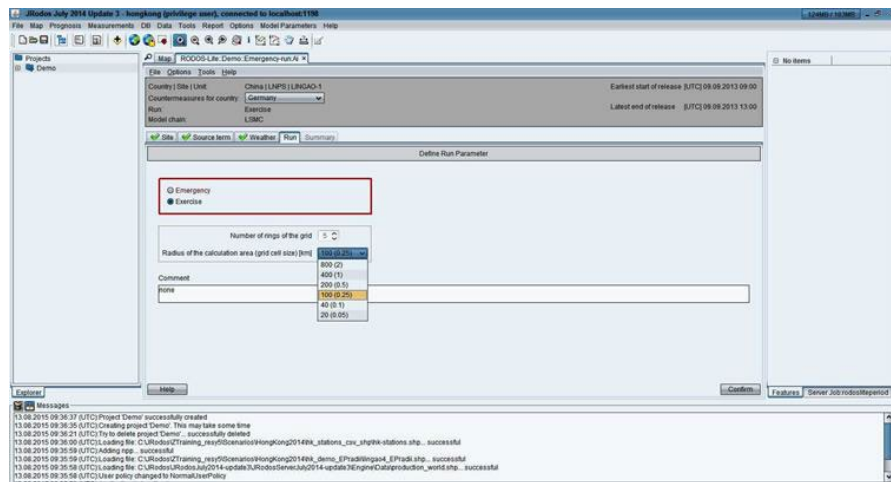
In the "Weather" tab (Figure A5-4), and in the in the "Prognosis time setup", we indicate the prognosis coverage after the beginning of the release, and the time steps of the outputs. Because the system is pre-configured to use the NOMADS data, it recognises that data are present for the specified prognosis period and allows proceeding to the next tab "Run".

**Figure A5-4.** Selection of the weather dataset.



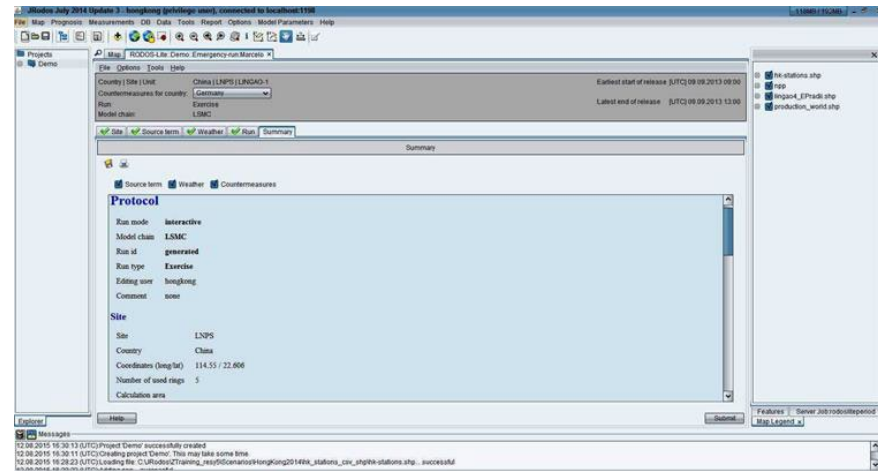
In the "Run" tab (Figure A5-5), one can select the grid type and the distance to which the calculation shall be performed. The chosen radius of calculation is 800 km, corresponding to a minimum grid cell size of 2 km. By default, JRODOS used 5 rings of the grids. This means that the grid cell size is 2 km around the point of release, and it becomes progressively coarser with the distance.

**Figure A5-5.** User input with RODOS-Lite; tab "Run".



Tab "Summary" (Figure A5-6), of which the screen dump shows only the uppermost part, gives a summary of the input. The operator studies the summary and clicks on [Submit] to start the calculation.

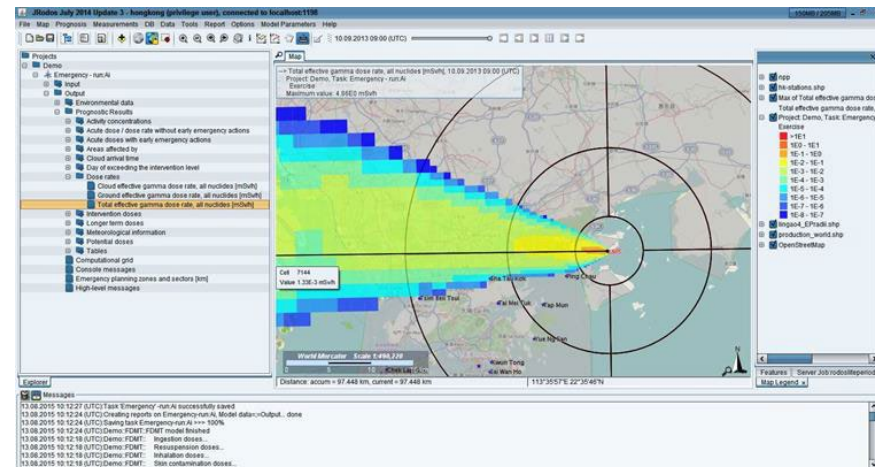
**Figure A5-6.** User input with RODOS-Lite; tab "Summary".



After submitting, prognostic calculations with the near range Atmospheric Transport and Deposition Model, the Emergency Action Simulation model and the Terrestrial Food Chain and Dose Module, are carried out one after the other, without further user interference. On the quad core notebook producing the demonstration screenshots, this took 5 minutes.

Figure A5-7 shows the JRodos User Interface and illustrates the presentation of map-type results. The central "Map" tab in Figure A5-7 consists of one or more result and map layers. The list of all layers in the Map tab, the "Map Legend", is visible to the right. The available results are offered in form of a "Result Tree" in the "Projects" section of the user interface to the left of the Map tab. From the "Result Tree", the operator can select the different results provided by the simulation of the specified source term and meteorological data.

**Figure A5-7.** JRodos User Interface; presentation of a map-type result (on OpenStreetMap).



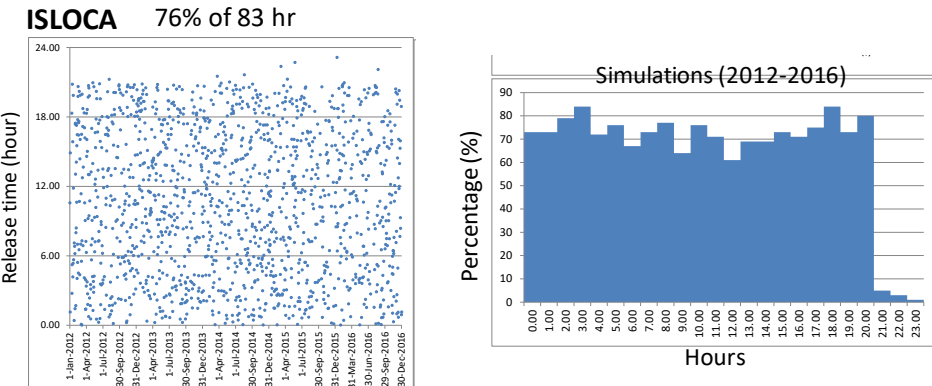
The total number of simulations were interactively generated by JRODOS. JRODOS provides a “statistic tool” for generating statistically distributed results for further analysis with external tools. The code generates a number of xml files and performs the calculations in a batch-job-like manner, without user interaction, by placing a bulk of the xml files (with the complete user inputs) in a certain directory. From there, they are automatically picked up by the system, the calculations are carried out and the generated results are saved; this feature is particularly attractive when the calculation times become bothersome.

Based on this statistic tool of JRODOS, an automated process was launched considering the meteorological sequence of the NCEP-GFS meteorological files and each source term independently:

- One daily release during the five year period 2012-2016;
- Starting time of the simulation: It was set by using the algorithm implemented in JRODOS for generating statistically distributed results within a previous defined period. In the reference period of this analysis, this algorithm uses 3000 starting hours. Figure A5-8. shows the temporal distribution of the starting times of runs for each source term, as well as the frequency of occurrence of the hours for the total

period of 5 years. Considering this distribution, the different seasons or months of the year are sampled, as well as the different times of the day; not too much variability in the time intervals between subsequent releases have been obtained. Note that deviations from homogeneous distribution are small considering the whole period, but only from 00:00 to 20:00 UTC. There is a decrease in the frequency of occurrence of releases in the last three hours of the day (from 21:00 to 23:00). In this sense, the JRODOS statistic tool would not fulfil the need to equally sample the different times of the day. This condition is needed because convective precipitation and atmospheric stability have characteristic diurnal variations. This is an inconvenience to be considered in the analysis of the results.

**Figure A5-8.** Hourly distribution of the starting hour of the 1825 plumes simulated for ISLOCA source term, and frequency of occurrence of the hours of the day for the starting times of runs.



## Reference

Karlsruhe Institute of Technology (KIT), 2017. JRodos Customer Guide. Version 3.0. February 2017. Page 24.

## Annex 6 Post-processing and visualization of the results from JRODOS

Due to the large number of results obtained a procedure to read the information has been designed. In JRODOS, the navigation to model results is performed via browsing through a “Result Tree” which represents the individual calculation results as “leaves” in folders and subfolders. The total number of available results can be huge, depending on the generating physical model. A “map view” visible in the JRODOS Main Window Tab, consists of a combined display of one or more layers of geo-referenced information, including map-type calculation results.

The procedure to read the information provided by the model is the following. For each simulation, the predictions for each output parameter were exported as ASCII tab delimited files (Figure A6-1). In every file, each grid cell is identified by a unique identification code (first column in Figure A6-1), while the following columns include the corresponding simulated values of the specific output parameter for each grid cell on hourly basis.

**Figure A6-1.** Example of one ASCII file.

Grid cell code	Simulation hours						
	1	2	3	4	5	6	7
0	0.0	0.0	0.0	0.0	0.0	0.0	0.0
1	0.0	0.0	0.0	0.0	0.0	0.0	0.0
2	0.0	0.0	0.0	0.0	0.0	0.0	0.0
3	0.0	0.0	0.0	0.0	0.0	0.0	0.0
4	0.0	0.0	0.0	0.0	0.0	0.0	0.0
5	0.0	0.0	0.0	0.0	0.0	0.0	0.0
6	0.0	0.0	0.0	0.0	0.0	0.0	523.9178
7	0.0	0.0	0.0	0.0	0.0	0.0	5116.3
8	0.0	0.0	0.0	3138.3362	3138.762		
9	0.0	0.0	0.0	6816.246	10018.187		
10	0.0	0.0	0.0	350.74847	12937.649		
11	0.0	0.0	0.0	0.0	539.0034	1272.197	
12	0.0	0.0	0.0	0.0	0.0	0.0	0.0
13	0.0	0.0	0.0	0.0	0.0	0.0	0.0
14	0.0	0.0	0.0	0.0	0.0	0.0	0.0
15	0.0	0.0	0.0	0.0	0.0	0.0	0.0
16	0.0	0.0	0.0	0.0	0.0	0.0	0.0
17	0.0	0.0	0.0	0.0	0.0	0.0	0.0
18	0.0	0.0	0.0	0.0	0.0	0.0	0.0
19	0.0	0.0	0.0	0.0	0.0	0.0	0.0
20	0.0	0.0	0.0	0.0	0.0	0.0	0.0
21	0.0	0.0	0.0	0.0	0.0	0.0	0.0
22	0.0	0.0	0.0	0.0	0.0	0.0	0.0
23	0.0	0.0	0.0	0.0	0.0	0.0	0.0
24	0.0	0.0	0.0	0.0	0.0	0.0	0.0
25	0.0	0.0	0.0	0.0	0.0	0.0	0.0
26	0.0	0.0	0.0	0.0	0.0	0.0	1090.859
27	0.0	0.0	0.0	8.780846	8.780846		
28	0.0	0.0	35.374146	4797.5815	4797.581		
29	0.0	0.0	0.0	8538.891	8755.257		
30	0.0	0.0	0.0	2645.0645	12571.697		
31	0.0	0.0	0.0	1.6723329	2029.8191		
32	0.0	0.0	0.0	0.0	0.0	0.0	0.0
33	0.0	0.0	0.0	0.0	0.0	0.0	0.0
34	0.0	0.0	0.0	0.0	0.0	0.0	0.0
35	0.0	0.0	0.0	0.0	0.0	0.0	0.0
36	0.0	0.0	0.0	0.0	0.0	0.0	0.0
37	0.0	0.0	0.0	0.0	0.0	0.0	0.0
38	0.0	0.0	0.0	0.0	0.0	0.0	0.0
39	0.0	0.0	0.0	0.0	0.0	0.0	0.0

In the consequence assessment of nuclear accidents, the parameters resulting from the calculations and used in the assessment are referred to as so-called endpoints of the calculations. Under ANURE, there are contamination and dose endpoints. In detail, for each one of the 1383 plumes generated, an ASCII tab delimited file was generated for each of the following endpoints:

- Ground contamination with  $^{131}\text{I}$ ,  $^{137}\text{Cs}$  and  $^{90}\text{Sr}$  at the end of the simulation respectively ( $\text{Bq m}^{-2}$ ).
- Total effective dose and inhalation dose (Sv).

From this kind of model simulation results, various post-processing tasks were needed to be done to achieve the project’s goals. This included conducting checks on missing hourly values on the results, producing graphical outputs in the form of maps, and various aggregation of output.

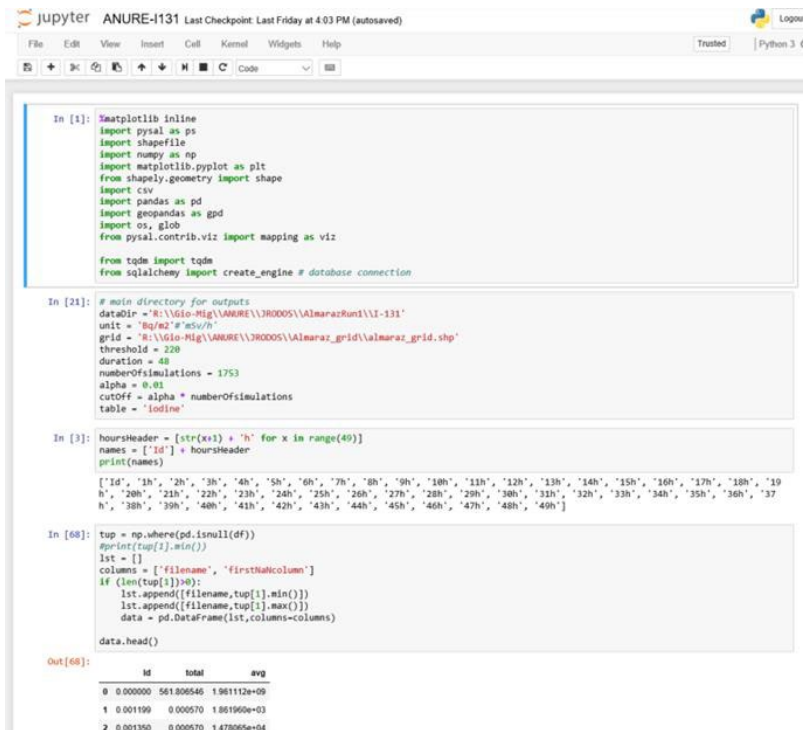
The first task accomplished after was to read and parse simulations, in csv files, and storing them in a relational database, notably SQLite DB ([www.sqlite.org](http://www.sqlite.org)). Two different tables were designed for storing separately  $^{131}\text{I}$ ,  $^{137}\text{Cs}$  and  $^{90}\text{Sr}$  deposition values, and total effective dose.

The main processing of these raw data was carried out using Python 3.6.2 in Jupyter notebook (<http://jupyter.org>). Several Python scripts were written and used for different purposes (Figure A6-2), such as statistical analysis of the modelling results. From each data set ( $^{131}\text{I}$ ,  $^{137}\text{Cs}$  and  $^{90}\text{Sr}$ ) the following results were obtained that were used in the next steps of the deposition mapping methodology:

- Maximum, minimum, average and percentiles of each grid cell;
- Frequency of each cell of being affected by the deposition;

- Frequency of exceedance for certain threshold of ground contamination.
- Frequency of exceedance for certain threshold of doses.

**Figure A6-2.** Screen shot of the Python script developed for ANURE.



The screenshot shows a Jupyter Notebook window titled "Jupyter ANURE-I131 Last Checkpoint: Last Friday at 4:03 PM (autosaved)". The notebook has three cells:

- In [1]:** Contains imports for Matplotlib, psal, shapefile, numpy, matplotlib.pyplot, shapely.geometry, csv, geopandas, os, glob, psal.contrib.viz, tqdm, and sqlalchemy.
- In [21]:** Contains variable definitions for unit, grid, threshold, duration, number\_of\_simulations, alpha, cutoff, and table. It also defines hoursHeader and names lists.
- In [68]:** Contains code to find min and max values for each column, create a list of tuples, and then create a DataFrame from these tuples.

**Out [68]:**

	Id	total	avg
0	0.000000	561.006546	1.981112e+09
1	0.001199	0.000570	1.861960e+03
2	0.001350	0.000570	1.478065e+04

Finally, shapefiles were created in which each grid cell contains the set of statistical values mentioned above as attributes. The visualisation of the results was carried out using Geographical Information Systems (GIS). There are many platforms to work with them, but in ANURE the one used is Quantum GIS (QGIS) (<https://qgis.org/en/site/>).

## **GETTING IN TOUCH WITH THE EU**

### **In person**

All over the European Union there are hundreds of Europe Direct centres. You can find the address of the centre nearest you online ([european-union.europa.eu/contact-eu/meet-us\\_en](http://european-union.europa.eu/contact-eu/meet-us_en)).

### **On the phone or in writing**

Europe Direct is a service that answers your questions about the European Union. You can contact this service:

- by freephone: 00 800 6 7 8 9 10 11 (certain operators may charge for these calls),
- at the following standard number: +32 22999696,
- via the following form: [european-union.europa.eu/contact-eu/write-us\\_en](http://european-union.europa.eu/contact-eu/write-us_en).

## **FINDING INFORMATION ABOUT THE EU**

### **Online**

Information about the European Union in all the official languages of the EU is available on the Europa website ([european-union.europa.eu](http://european-union.europa.eu)).

### **EU publications**

You can view or order EU publications at [op.europa.eu/en/publications](http://op.europa.eu/en/publications). Multiple copies of free publications can be obtained by contacting Europe Direct or your local documentation centre ([european-union.europa.eu/contact-eu/meet-us\\_en](http://european-union.europa.eu/contact-eu/meet-us_en)).

### **EU law and related documents**

For access to legal information from the EU, including all EU law since 1951 in all the official language versions, go to EUR-Lex ([eur-lex.europa.eu](http://eur-lex.europa.eu)).

### **Open data from the EU**

The portal [data.europa.eu](http://data.europa.eu) provides access to open datasets from the EU institutions, bodies and agencies. These can be downloaded and reused for free, for both commercial and non-commercial purposes. The portal also provides access to a wealth of datasets from European countries.

# Science for policy

The Joint Research Centre (JRC) provides independent, evidence-based knowledge and science, supporting EU policies to positively impact society



**EU Science Hub**

[joint-research-centre.ec.europa.eu](http://joint-research-centre.ec.europa.eu)



Publications Office  
of the European Union